LBL-26220
UC-411

Lawrence Berkeley Laboratory
UNIVERSITY OF CALIFORNIA

Accelerator & Fusion Research Division

RECEIVED
LAWRENCE
BERKELEY LABORATORY

JUL 3 1989

LIBRARY AND
DOCUMENTS SECTION

Center for X-Ray Optics

A Method for Sizing Sub-micron Particles Using Small Angle Diffraction of Soft X-Rays

D.J. Berkeland, J.H. Underwood, and R.C.C. Perera

October 1988

TWO-WEEK LOAN COPY

This is a Library Circulating Copy which may be borrowed for two weeks.

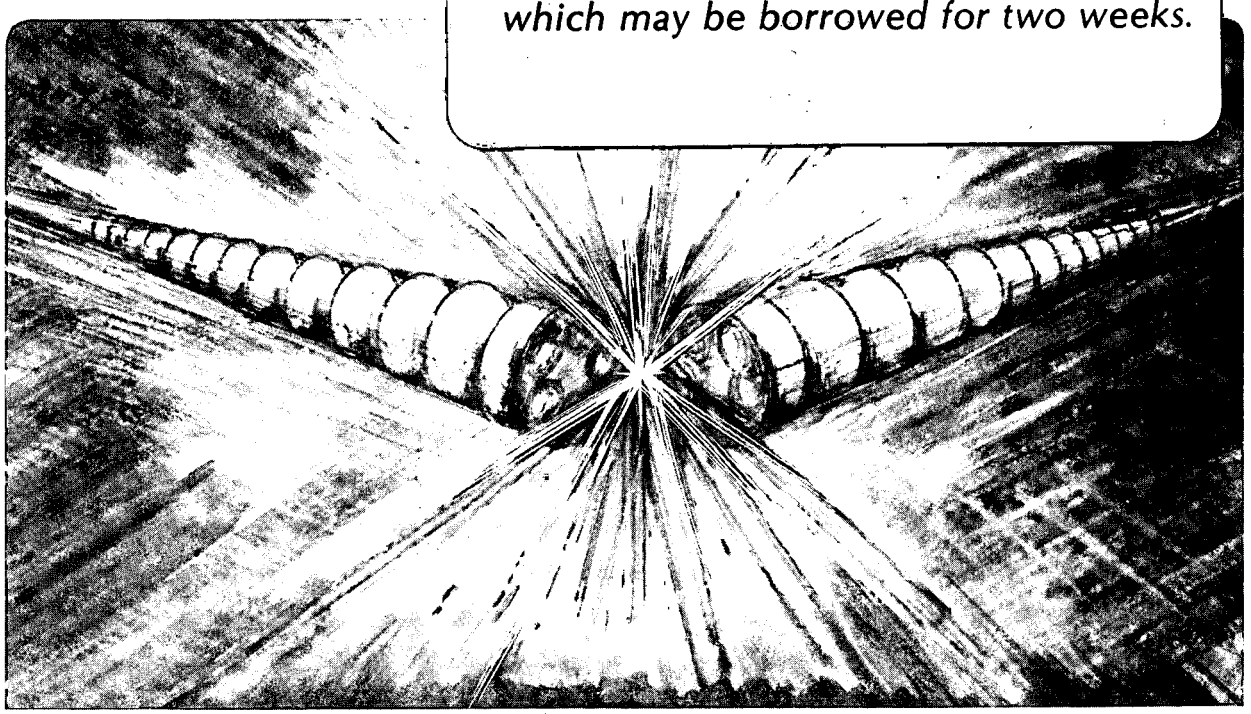

LBL-26220 c.2

Prepared for the U.S. Department of Energy under Contract Number DE-AC03-76SF00098.

DISCLAIMER

This document was prepared as an account of work sponsored by the United States Government. While this document is believed to contain correct information, neither the United States Government nor any agency thereof, nor the Regents of the University of California, nor any of their employees, makes any warranty, express or implied, or assumes any legal responsibility for the accuracy, completeness, or usefulness of any information, apparatus, product, or process disclosed, or represents that its use would not infringe privately owned rights. Reference herein to any specific commercial product, process, or service by its trade name, trademark, manufacturer, or otherwise, does not necessarily constitute or imply its endorsement, recommendation, or favoring by the United States Government or any agency thereof, or the Regents of the University of California. The views and opinions of authors expressed herein do not necessarily state or reflect those of the United States Government or any agency thereof or the Regents of the University of California.

A Method for Sizing Sub-micron Particles Using Small Angle Diffraction of Soft X-Rays

Dana J. Berkeland,
James H. Underwood
and
Rupert C.C. Perera

Center for X-Ray Optics
Acclerator and Fusion Research Division
Lawrence Berkeley Laboratory
1 Cyclotron Road
Berkeley, CA 94720

Contents

Abstract 1

Introduction 2

Theory

A: Scattering from a Single Particle 6

B: Scattering from an Ordered Array of Particles 12

Experimental

A. Calculation of Index of Refraction 20

B. Window Material and its Effects 22

C. Film Characteristics 25

D. Reflection from a Multi-layer Mirror 27

E. The Diffracting Samples 28

F: The X-Ray Source 32

G: The Pinhole Collimation Device 36

H: The Multi-layer Mirror Device 40

Conclusion 61

Acknowledgements 62

Appendix 1 63

Appendix 2 67

References 70

Abstract

The purpose of this work is to develop a method of sizing sub-micron particles using small-angle soft x-ray diffraction. Solid poly-styrene spheres of known sizes were used as scattering samples, with C-Kα (44.8Å) and V-Lα (24.3Å) radiation from a conventional x-ray source. Two devices were used to diffract the x-rays. One collimates the radiation using a series of pinholes immediately preceding the sample, and directs the unfocussed radiation onto film placed far from the sample. The other utilizes radiation from a single pinhole above the source onto the sample and a spherical multilayer mirror in series, so that the radiation passes twice through the sample and is focussed onto film immediately above the pinhole assembly to increase the effective sample area. Using the latter device, two types of diffraction patterns were obtained: a sharp, relatively small pattern from spheres which form a hexagonal lattice structure, and a diffuse, larger pattern from an unordered, or random, array of spheres. Both patterns are presented in this work, along with the calculations, based upon light scattering from an unordered and an ordered array of particles, of the scattering patterns.

Introduction

This work illustrates a method of observing sub-micron particles (e.g. biological particles such as zymogen granules) not only without destroying or altering the particles but also while allowing the particles to exist in a controllable or natural environment. Methods of sizing sub-micron particles have existed for years, using electron microscopy, ultra-violet light and x-ray scattering. The electron microscope produces fine images of sub-micron samples, but at the cost of altering the sample, to a significant or unknown extent, during preparation, while under vacuum, or while under electron bombardment. Further, the requirement for a vacuum prohibits the interesting experiments which control the environment of the sample. While the UV light scattering method allows such experiments, and generally does not alter the sample, it has the difficulty that for particles of sub-micron size and smaller, the scattering pattern subtends a wide angular range. Relatively complicated devices containing moving detectors must be utilized to obtain a pattern whose shape may not be very revealing.

Diffraction patterns of radiation in the soft x-ray region are small enough that a single piece of 35mm film can record the pattern. The sample may be kept under a low vacuum, so that its environment may be controlled. Henke[1] presented several possible arrangements for detecting small angle scattering patterns in the x-ray region, and these are shown in Figure 1. Figures 1(a)-(c) illustrate devices which allow detection of radiation scattered at relatively large angles, that is, from particles of sizes on the order of the radiation wavelength. Like the devices which detected UV scattered radiation patterns, these devices employ movable device components (detector, crystal). Figures 1(d) and (e)

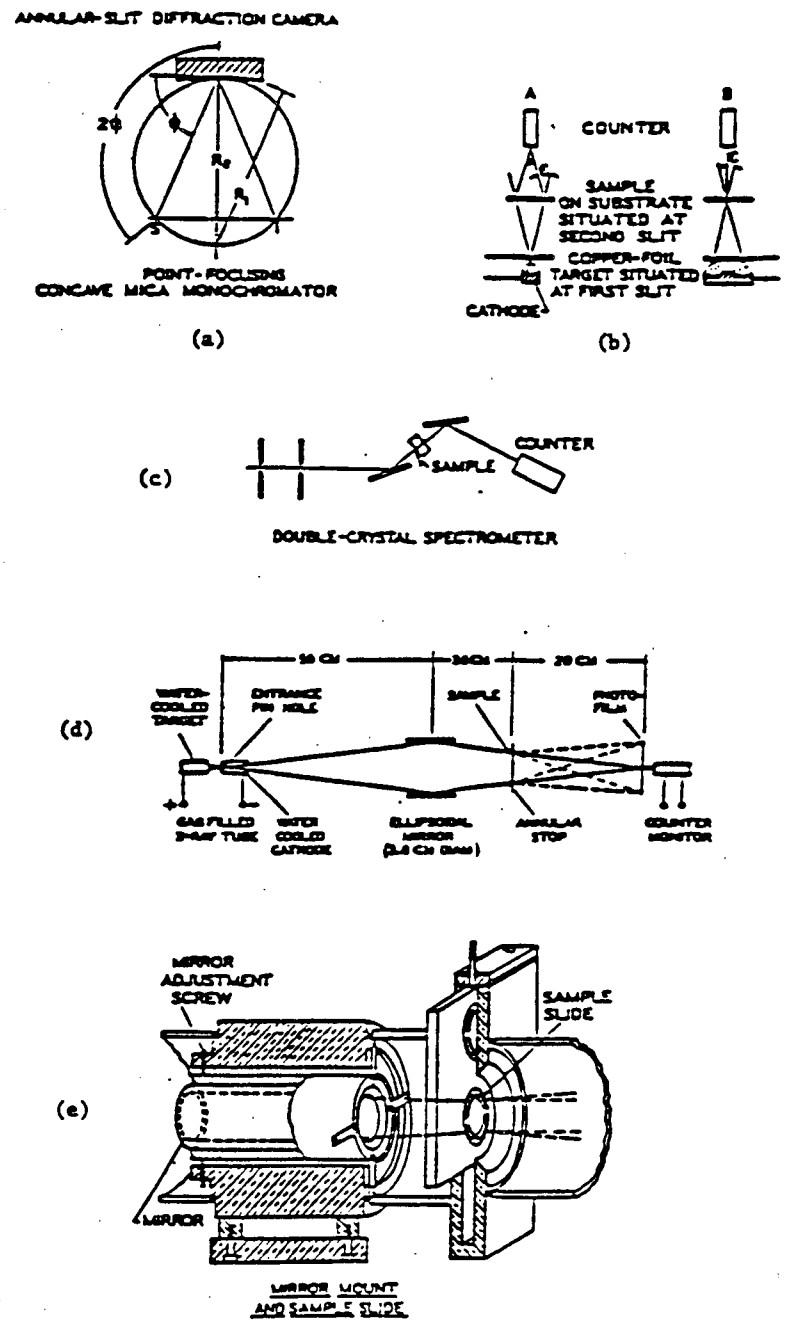

Figure 1: Four types of x-ray beam geometries used for the measurement of diffraction patterns.

illustrate the total reflection camera, which is the most similar of these devices to the device presented in this work in that unscattered radiation is focussed to a point at the detector (film, in both cases). Radiation is reflected at grazing incidence by an ellipsoidal mirror onto a portion of a scattering sample. The radiation arriving at the film is focussed to a point in the absence of a scattering sample, only a small annular region of the radiation is transmitted through the sample location, as shown in Figure 1(e). Thus only the sample in that annular region contributed to the scattering pattern. But in addition to the general problem with using x-rays to size particles, i.e., that the extremely high energy flux of the x-rays may destroy a biological sample, the exposure times necessary to obtain an observable scattering pattern even with the total focussing camera are extremely long (around 20 hours) because the area of sample which was illuminated by the radiation was relatively small.

This work offers a solution to these problems by using a pinhole to image an extended source onto a normal incidence multi-layer mirror. In addition to using x-rays of relatively low energy, the diffracted beam is broadened at the sample location, so that the flux of x-rays at the sample is lower than at the source. Thus the particles are not necessarily subject to destructively high radiation fluxes. The low photon flux at the sample is accounted for by the fact that, since a large area of the sample is illuminated, many particles of the sample contribute to the observed scattering of radiation, resulting in a diffraction pattern of measurable intensity. To emphasize this, a device which illuminates only a small area of a sample[2], and fails to obtain a diffraction pattern, is presented in this work.

This work utilizes polymer spheres of sub-micron

diameter. The size of the diffracting particles is known for calibration purposes, and the results are not affected by changes in the sample during the exposure. The next step in this work is to use a sample of biological particles (e.g. zymogen granules) in the apparatus and to size the granules. Ultimately, the method presented here may be modified to included a separate, low vacuum, chamber for the diffracting sample, that allows the environment of the sample to be controlled. Calculations presented here may be extended to include non-spherical particles and particles of non-uniform size and density. Then, important information about many other biological particles, such as their size, shape, and internal structure, may be obtained.

Theory

A: Scattering from a Single Particle

The assumptions made in this experiment are that the particles are spherical, with uniform density and index of refraction very close to unity, and of radius very large compared to the wavelength of the radiation[3]. The first two assumptions determine the geometry of the problem; the third permits neglecting refraction effects within the particle; the last allows one to use geometrical optics within the particle.

Consider the situation in Figure 2, of a sphere of radius a and complex index of refraction $m = 1 - (\delta + i\beta)$, where δ and β are real quantities. In the x-ray region both δ and β are small and positive for a vacuum/material interface. The initial wave is a plane wave with disturbance ψ_o. Call k the wave number, i.e. $k = 2\pi/\lambda$. A ray passing through the sphere at an angle τ suffers a phase shift of

$$\phi = \delta\ k\ (2a \sin\tau)$$

and an attenuation of

$$\exp\ [\ -\ \beta\ k\ (2a \sin\tau)]\ .$$

When refraction effects are neglected, the disturbance ψ in the plane immediately above the sphere, that is, within the geometrical shadow area of the sphere (see Figure 2), is

$$\psi = \psi_o \exp[2ka\ i\ (\delta + i\beta) \sin\tau\ ]$$

and $\psi = \psi_o$ outside of the geometrical shadow area. Substituting

$$\rho = -2ka(\delta + i\beta) = 2ka\ (m - 1)\ ,$$

we can write

$$\psi = \psi_o \exp\ (-\ i\rho \sin\tau\ )$$

inside the shadow area. Alternatively, the disturbance

$$\psi_1 = \psi_o\ [\exp\ (-\ i\rho \sin\tau) - 1]$$

has been added to the initial plane wave disturbance.

A plane in which the disturbance is ψ_o everywhere

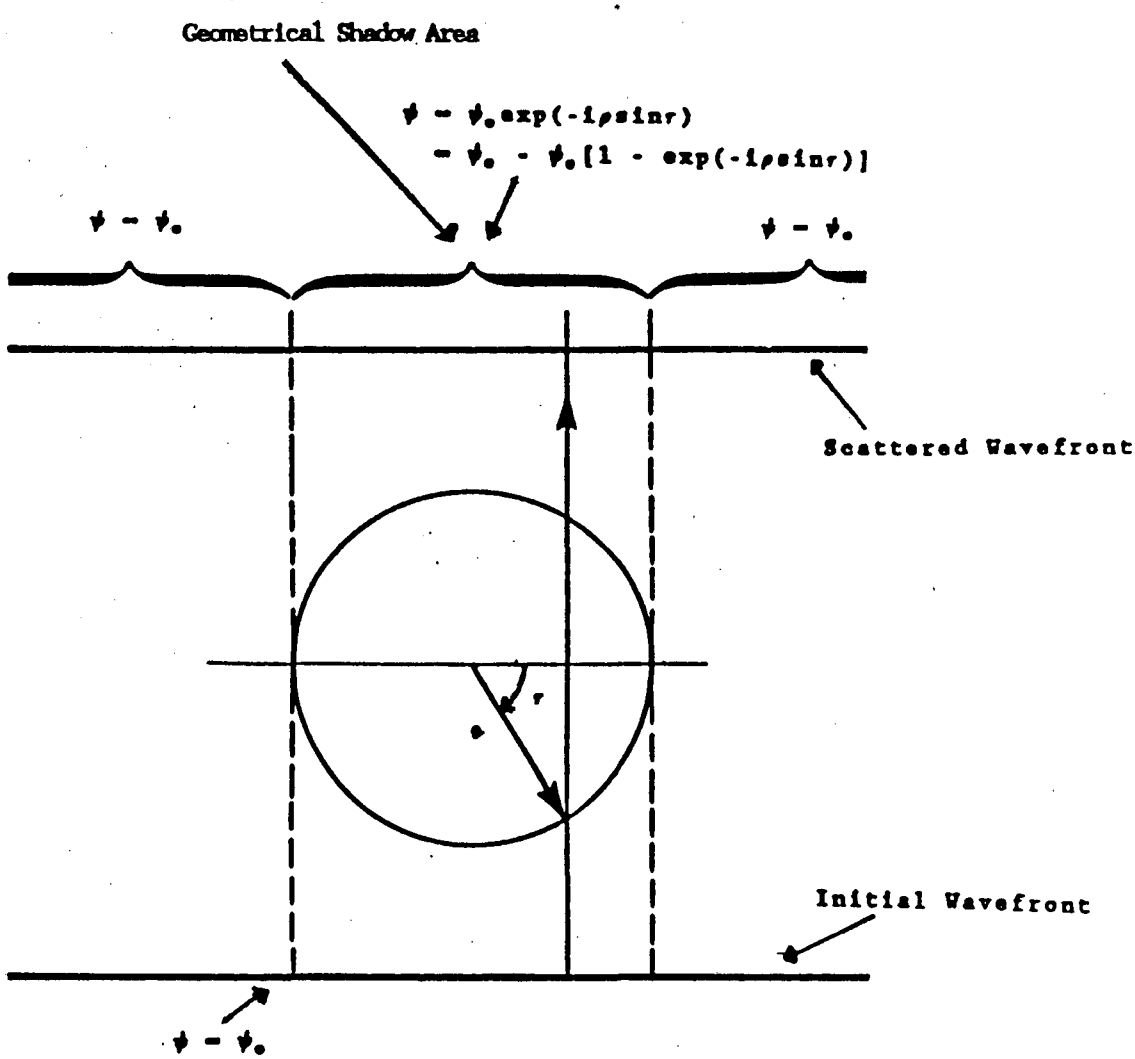

Figure 2: Radiation passing through a sphere

except for in the shadow area, where it is ψ, is conjugate to a plane in which the disturbance is zero outside of the shadow area, where it is ψ_o. That is, if the disturbances of the two planes are added, the total disturbance is ψ_o. According to Babinet's principle[4], the disturbance at any point resulting from the disturbance of the first plane is equal in magnitude and negative in sign to the disturbance from the second plane, if the plane wave may be neglected. This is the case if the resultant wave is focussed so that the plane wave (unscattered) components are separated from the scattered components.

Hence, using the Huygens-Fresnel principle[4], the disturbance at a point P at position **r** arising from the differential area dA at position **r'** in the shadow area is

$$d\psi = -\ (ik/2\pi r)\ \tfrac{1}{2}\ (1 + \cos\theta)\ \psi_1\ \exp[-ik|\mathbf{r} - \mathbf{r}'|]\ dA$$

In the region that $r >> r'$, we can make the approximation

$$|\mathbf{r} - \mathbf{r}'| \sim r - \hat{\mathbf{r}}\cdot\hat{\mathbf{r}}'\ r'$$

$$= r - (\sin\theta\ \cos\phi\ \cos\emptyset + \sin\theta\ \cos\phi\ \sin\emptyset)\ r'$$

where the angles θ, ϕ, and $\emptyset$ are as shown in Figure 3. Thus the disturbance at P from dA is

$$d\psi = (ik/2\pi r)\ \tfrac{1}{2}\ (1 + \cos\theta)\ \exp(-ikr)\ [1 - \exp(-i\rho\sin\tau)]$$
$$* \exp[ik\ \sin\theta\ \cos\phi\ (\cos\emptyset + \sin\emptyset)\ r']\ r'\ dr'd\emptyset$$

The total disturbance at P is the integral of the disturbances from differential areas of the shadow area. From symmetry, the disturbance at P will have no dependance on ϕ, so that the $\cos\phi$ terms may be ignored, and in the limit that θ is very small, the total disturbance is

$$\psi = (ik/2\pi r)\ \exp(-ikr) \int \{r'\ dr'\ d\emptyset\ [1 - \exp(-i\rho\sin\tau)]$$
$$* \exp[ik\theta\ (\cos\emptyset + \sin\emptyset)\ r']\ \}$$

Changing the variables

$$x = a\ \cos\tau\ \cos\emptyset$$
$$y = a\ \cos\tau\ \sin\emptyset$$

such that

$$dx\ dy = a^2 \cos\tau\ \sin\tau\ d\tau\ d\emptyset$$

and defining

$$z = ka\theta\ ,$$

then the integral becomes

$$\psi = (ik\psi_o/2\pi r)\ \exp(-ikr) \int \{\ [1 - \exp(-i\rho \sin\tau)]\ \cos\tau\ \sin\tau\ d\tau$$
$$* \int \exp(-iz\ \cos\tau\ \cos\emptyset)\ d\emptyset\ \}$$

The integral over $\emptyset$ is equal to $2\pi J_o(z\ \cos\tau)$, where J_o is the Bessel function of order 0. Thus the integral is equal to

$$\psi = (ik\psi_o/r)\ \exp(-ikr) \int \{\ [1 - \exp(-i\rho\ \sin\tau)]$$
$$* J_o(z\ \cos\tau)\ \cos\tau\ \sin\tau\ d\tau\ \}$$

In this experiment, the incident light passes twice through the sphere--before and after the light is reflected from the mirror (see experimental section). The above calculations still apply to this situation, but in the integral, ρ is replaced by 2ρ. The intensity at point P is $\psi^*\psi$, and this is calculated numerically. (See Appendix 1 for a print-out of this program which performs these calculations.)

In order to obtain a scattering pattern qualitatively equal to that of a single sphere but greater in intensity, a scattering sample of a thin layer of many spheres in an unordered array should be used. When considering scattering by a random array of identical spheres, the amplitude function of every sphere is equivalent and, more importantly, incoherent of the other spheres. Hence the intensity pattern of scattered light from such an array of total N spheres will be approximately identical to that of a single sphere, with magnitude NI (r), where I (r) is the intensity at r of light scattered from a single particle.

Even if the sample contains spheres which vary slightly in diameter, the expected diffraction pattern from each sphere is still approximately the same, and the size of the total diffraction pattern should be the

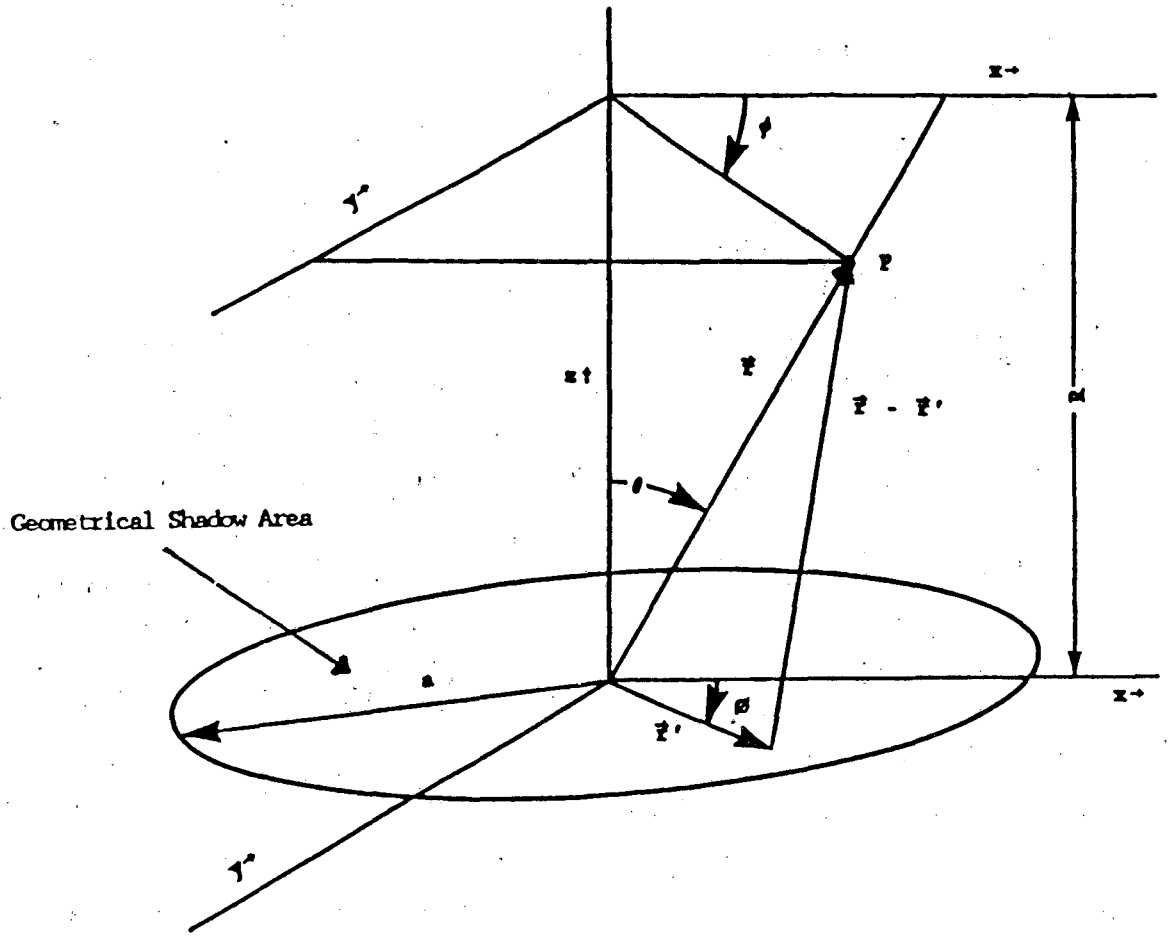

Figure 3: Geometry of the diffraction of radiation by a sphere (distances grossly exaggerated).

average of the sizes of those from each sphere; hence for a sample which contains spheres of a small diameter distribution the diffraction pattern will be roughly the diffraction pattern of a single sphere whose diameter is that of the average diameter of the spheres.

B: Scattering from an Ordered Array of Particles

The effect of interparticle interference on the experimental results is significant, changing not only the size but the shape of the intensity distribution of the scattered light. While most experiments in light scattering from small particles assume a random distribution of particles and hence a diffraction pattern of the same size and shape as a single particle scattering pattern, the probability of (unknowingly) producing an ordered array of particles is large enough to warrant discussion of the situation.

The most probable lattice structure of a close-packed array of spherical particles is hexagonal, as shown in Figures 4, 5, and 6. Initially the array may be treated as a set of point sources located at the centers of the spheres, and thought of as a set of crossed diffraction gratings (ultimately, however, it must be treated as a phase grating). A set of crossed diffraction gratings will produce a pattern which is the interference pattern of the set of gratings; this pattern will be a set of sharp maxima which are discrete peaks rather that continuous lines. With this in mind, consider that sets of single lines which contain particle centers spaced 2a apart, where a is the radius of the spheres, as illustrated in Figure 4. The lines show a six-fold symmetry, and the distance between any two parallel lines is $3^{\frac{1}{2}}a$, which is the furthest distance possible between any set of parallel planes. The axial angles at which maxima occur from diffraction from a parallel set of these lines is then

$$\theta = \lambda/(3^{\frac{1}{2}}a) ,$$

where the grating equation for small angles has been used, and θ is the angle from the normal of the plane of the array. If the azimuthal angle ϕ is defined as shown in Figure 4, the maxima are expected to occur at

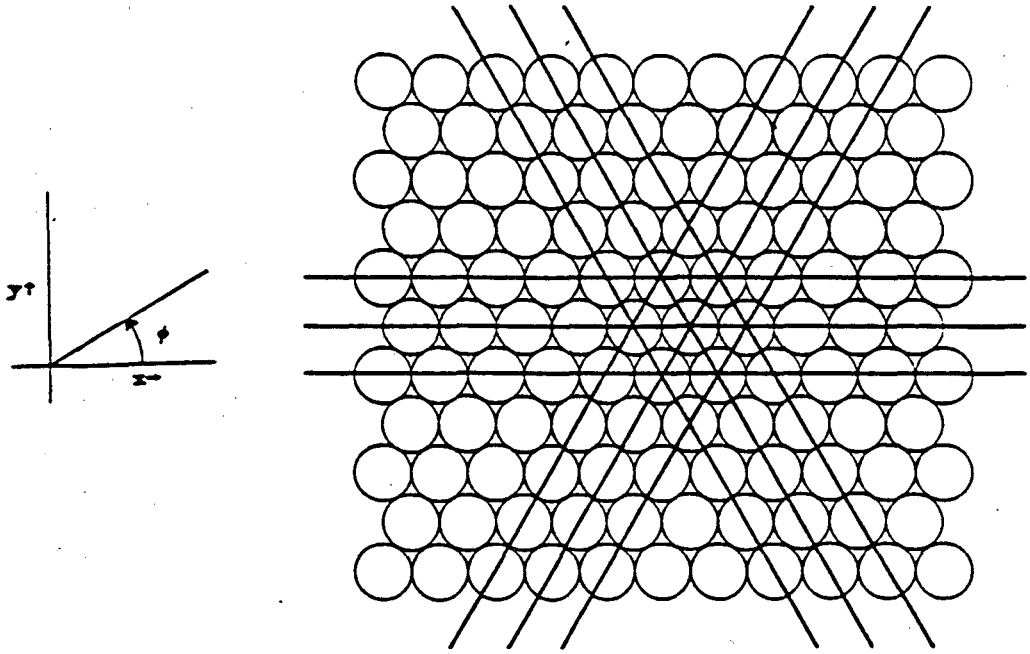

(a)

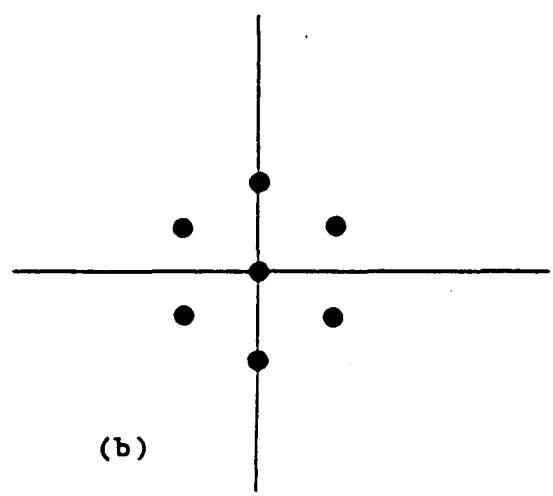

(b)

Figure 4

a) Lines of spacing $d = 2a\sin(\pi/3) = \sqrt{3}a$

b) Corresponding primary and secondary maxima pattern (not to scale)

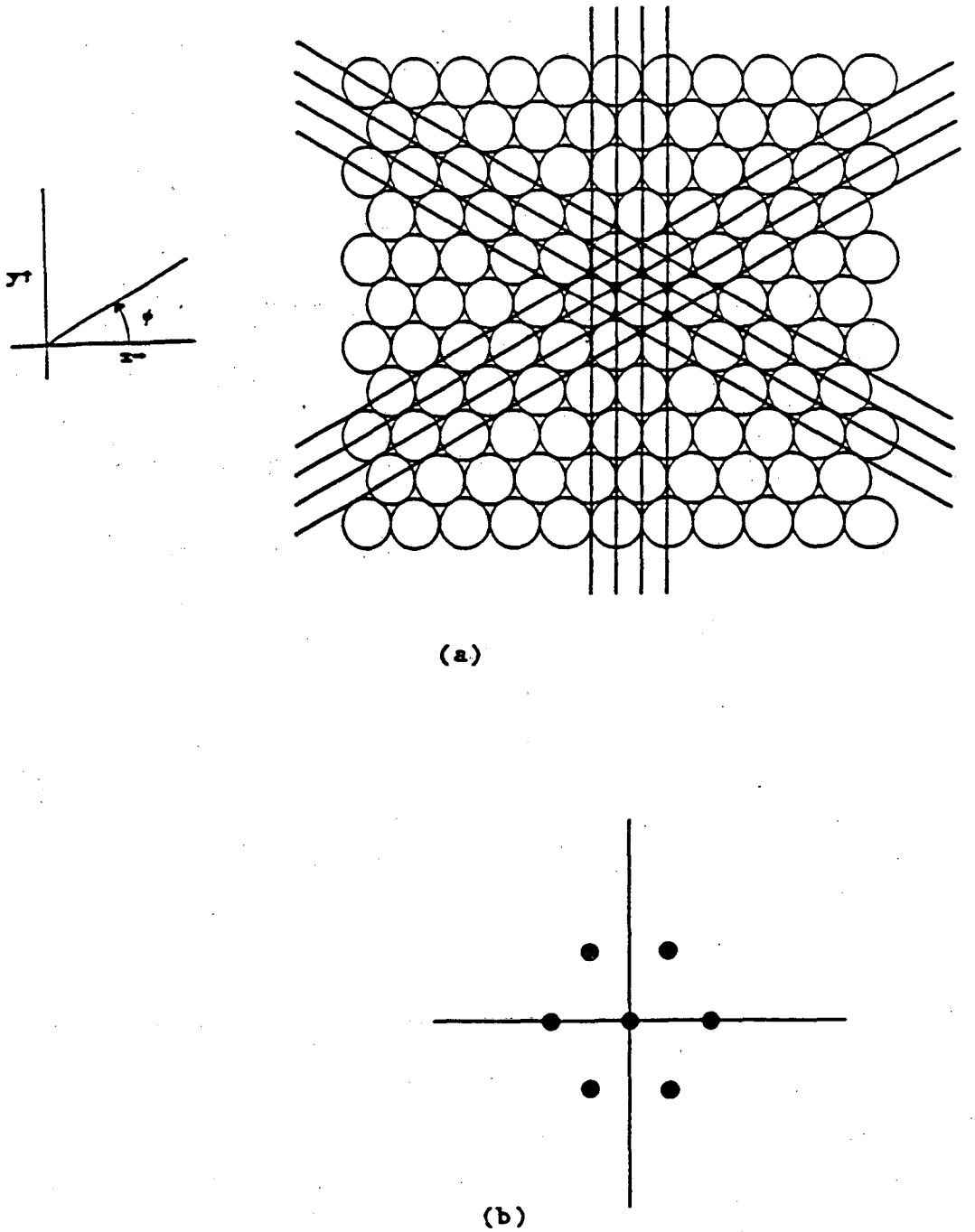

Figure 5

a) Lines of spacing $d = 2a\sin(\pi/6) = a$

b) Corresponding primary and secondary maxima pattern (not to scale)

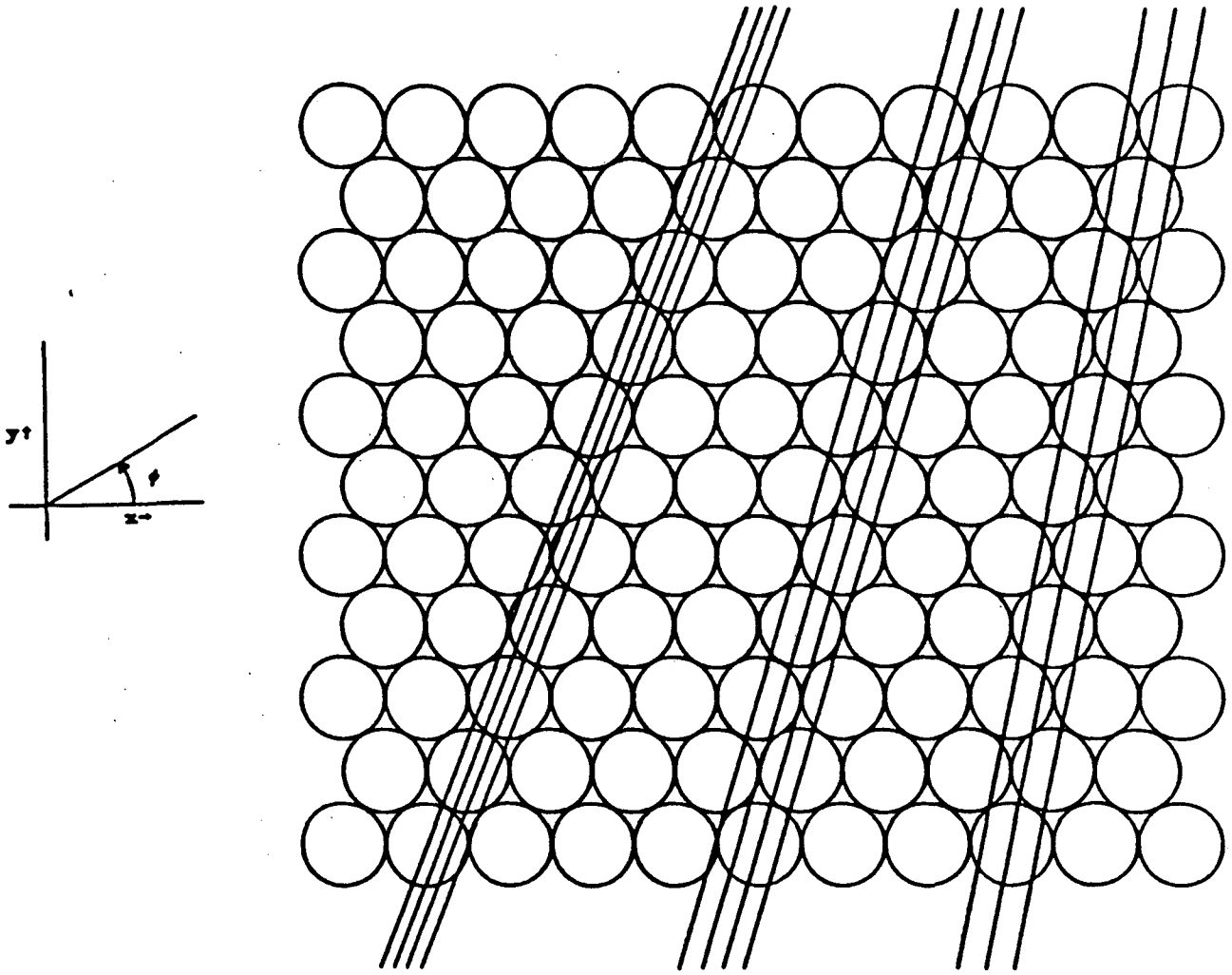

Figure 6: Lines of spacing $d = 2a\sin(\pi/48)$
$d = 2a\sin(\pi/24)$
$d = 2a\sin(\pi/12)$

$$\phi = (2m + 1)\ (\pi/6) \text{ where } m = 0,\ \pm 1,\ \pm 2$$

as these are the angles perpendicular to the parallel lines of spheres, because from symmetry arguments regarding the orientation of the other sets of parallel lines the maxima must occur at such angles.

The second largest spacing between two sets of parallel lines is $d = 2a \sin(\pi/6) = a$, for the set of lines shown in Figure 5. The maxima from these lines occur at

$$\theta = \lambda / a$$

and $$\phi = 2m\ \pi/2 = m\pi \quad \text{where } m = 0,\ \pm 1,\ \pm 2$$

Many sets of parallel lines may be drawn, with spacings of $d_n = 2a \sin(2^{-n}(\pi/3))$, where $n \geq 0$, as shown in Figure 6. Angles at which the corresponding m^{th} maxima occur are

$$\theta_{nm} = m\lambda / d_n$$

which shows that as the spacing between the parallel lines become smaller, the axial angle θ_{n1} of the first maximum becomes greater. For reasons which will be discussed later, because they occur at relatively large values of θ, these maxima (and also the secondary maxima) are attenuated so that they are no longer observable.

This method of approximation gives the angles at which maxima are expected, but it fails to give the relative intensities of maxima. As mentioned earlier, the array of spheres should be treated as a phase grating. This treatment shows that the intensity of light scattered from the array is the intensity of a set of point sources, as considered in the above arguments, but modulated by the intensity function of light scattered by a single sphere.

This is shown by first writing the disturbance at location r due to light scattered from a single particle at the origin as

$$\psi(\mathbf{r}) = (ik\psi_o/r)\ \exp(-ikr) \int \{\ [1 - \exp(-i\rho\sin\tau)]$$
$$* \ J_o(z\ \cos\tau)\ \cos\tau\ \sin\tau\ d\tau\ \}$$
$$= \psi_1(r,\ \theta)\ \exp(-ikr)$$

which defines $\psi_1(r,\ \theta)$ in this case. The expression is that from the previous section, but the equation

$$\psi(\mathbf{r}) = \psi_1(\mathbf{r})\ \exp(-ikr)$$

holds generally for any disturbance $\psi(\mathbf{r})$. The desired quality of $\psi_1(\mathbf{r})$ is that it be almost invariant under small changes in $\mathbf{r}$, unlike the exponential term which, because of the large value of k, may vary drastically with small changes in the magnitude of $\mathbf{r}$.

To find the disturbance at $\mathbf{r}$ from light scattered by a particle at position $\mathbf{r}'$, which is not at the origin, the coordinate system in the above equations is translated by the position $\mathbf{r}'$, so that the disturbance ψ_2 at $\mathbf{r}$ is

$$\psi_2(\mathbf{r}) = \psi(\mathbf{r} - \mathbf{r}') = \psi_1(\mathbf{r} - \mathbf{r}')\ \exp(\ -ik|\mathbf{r} - \mathbf{r}'|)$$

Given that $r'/r << 1$, and the ψ_1 is roughly invariant to small changes in $\mathbf{r}$, this can be written

$$\psi_2(\mathbf{r}) \sim \psi_1(\mathbf{r})\ \exp(-ik|\mathbf{r} - \mathbf{r}'|)$$

Next, $|\mathbf{r} - \mathbf{r}'|$ may be expanded and approximated as

$$|\mathbf{r} - \mathbf{r}'| \sim r - \mathbf{r}\cdot\mathbf{r}'/r$$

which gives

$$\psi_2(\mathbf{r}) \sim \psi_1(\mathbf{r})\ \exp(-ikr)\ \exp(ik\mathbf{r}\cdot\mathbf{r}'/r)$$
$$= \psi(\mathbf{r})\ \exp(ik\mathbf{r}\cdot\mathbf{r}'/r)$$

The exponential expression is the disturbance at $\mathbf{r}$ arising from a point source at location $\mathbf{r}'$. Considering an array of particles, each with an index i,j and located at the corresponding position $\mathbf{r}_{ij}$, the total disturbance at $\mathbf{r}$ is the sum of the disturbances of each particle:

$$\psi_3(\mathbf{r}) \simeq \psi(\mathbf{r}) \sum \exp(ik\mathbf{r}\cdot\mathbf{r}_{ij}/r) = \psi(\mathbf{r}) \sum \psi_{lat}$$

But outside of a factor of a constant divided by r, this is just the disturbance of a single particle multiplied by the disturbance of a lattice of point sources. Then

$$\psi_2(\mathbf{r}) \sim \psi(\mathbf{r})\ \psi_{lat}(\mathbf{r})$$

and the total intensity is

$$I_2(\mathbf{r}) = \psi_2^* \psi_2 \sim (\psi^* \psi)\ (\psi_{lat}^* \psi_{lat}) = I(\mathbf{r})\ I_{lat}(\mathbf{r})$$

where $I(\mathbf{r})$ is the single particle intensity pattern and $I_{lat}(\mathbf{r})$ is proportional to the intensity pattern of a two dimensional lattice. If the intensity pattern from a lattice has very sharp maxima and if, at these maxima, the single particle intensity varies slowly, the pattern from the lattice dominates the resulting intensity pattern. However, the peak value of the maximum intensities will be modulated by the intensity function of a single particle so that the maxima will vary in intensity with the axial angle θ, generally decreasing as θ increases.

To get a better idea of how the single particle intensity distribution modulates the lattice distribution, one can calculate the function $I_{lat}(\mathbf{r})$. Referring to Figure 6 and indexing the particles as x_{nm}, where n refers to the horizontal position of the particle and m refers to the vertical position, the position of any sphere is given by

$$\mathbf{r}_{nm} = na\ \hat{x} + 2ma \sin(\pi/3)\ \hat{y}$$
$$= na\ \hat{x} + 3^{1/2} ma\ \hat{y}$$

where $n = 0, 2, 4, 6, \ldots$ if m is even
$= 1, 3, 5, 7, \ldots$ if m is odd

By substituting these values into the expression for the lattice intensity and performing the summation by using the identity

$$\sum \exp(in\delta) = \exp[i\tfrac{1}{2}(N-1)\delta]\ \sin^2(\tfrac{1}{2}N\delta)\ /\ \sin^2(\tfrac{1}{2}\delta)$$

and $\mathbf{r} = \sin\theta\ \cos\phi\ \hat{x} + \sin\theta\ \sin\phi\ \hat{y} + \cos\theta\ \hat{z}$

and substituting $z = ka\sin\theta$, one obtains the expression

$$I_2(\mathbf{r}) = I(\mathbf{r})\ \sin^{-2}(z\ \cos\phi)\ \sin^{-2}(z\ \sin\phi\ 3^{1/2})\ )$$
$$* \sin^2[\tfrac{1}{2}(N+1)\ z\ \cos\phi]\ \sin^2[\tfrac{1}{2}(M+1)\ z\ \sin\phi\ 3^{1/2}]$$
$$* [1 + \cos(z\ \cos\phi + 3^{1/2} z\ \sin\phi)\ ]$$

where, in order to keep the expression simple, it is assumed that the array is rectangular, as in Figures 4, 5

and 6, but N and M, the indices of the final (corner) sphere, are assumed to be odd (this is not the case in Figures 4, 5, or 6).

The value of this expression can be calculated numerically for various angles. The intensity of first maximum at $\phi = \pi/6$ ($\theta = \lambda/3^{1/2}a$) is greater than that at $\phi = 0$ ($\theta = \lambda/a$) by approximately an order of magnitude. This maximum, in turn, is greater than the second maximum at $\phi = (\pi/6)$ ($\theta = 2\lambda/(3^{1/2}a)$) by approximately another order of magnitude. Subsequent maxima decrease rapidly in intensity as the single particle intensity drops in magnitude.

The observed scattering pattern will be from a sample of many randomly oriented arrays. The observed pattern will be the sum of many patterns of discreet maxima at random angles ϕ but at specific angles θ. Thus the observed scattering pattern will consist not of a set of discreet maxima but of a set of ring-shaped maxima at the same angles θ as the single array pattern maxima. This is analogous to a powder diffraction pattern in x-ray diffraction. As discussed earlier, the angles which will give the most intense maxima will be at $\lambda/(3^{1/2}a)$ and λ/a radians. The observance of any more maxima will depend on the sensitivity of the measurements.

Experimental

A: Calculation of the Index of Refraction

In this work the wave number k and the sphere diameter 2a have already been given. The final parameters are the indices of refraction, neccessary in determining the scattering pattern and the reflectivity of the spherical mirror (next section) and mass absorbtion coefficients, neccessary in determining the proper window material (next section).

The complex index of refraction $m = 1 - (\delta + i\beta)$ is determined by the formula

$$\delta \simeq (r_o/2\pi)\ \lambda^2 \phi \sum x_p f_{1p}$$

and

$$\beta \simeq (r_o/2\pi)\ \lambda^2 \phi \sum x_p f_{2p}$$

where r_o is the classical electron radius, λ the radiation wavelength, ϕ the number of molecular groups per unit volume, with x_p atoms of type p per molecular group. f_{1p} and f_{2p} are the real and imaginary components, respectively, of the atomic scattering factor of an atom of type p.

To calculate the index of refraction of polystyrene (of specific gravity 1.05 g cm^{-3} and formula $(C_6H_5CHCH_2)_x$) consider that the number of carbon atoms equals the number of hydrogen atoms and hence the number density of either atom is

$$\phi x_C = \phi x_H = N_A\ (1.05\ g\ cm^{-3})\ /\ (12.01g + 1.00g)$$
$$= 4.86 \times 10^{22}\ atoms\ cm^{-3}$$

where N_A is Avogadro's number. Using the values of the scattering coefficients[5] for C-Kα radiation (λ = 44.8Å),

$$f_{1H} = 1.01$$
$$f_{2H} = 3.06 \times 10^{-3}$$
$$f_{1C} = 0.99$$
$$f_{2C} = 0.186$$

one obtains the values

$$\delta = 8.75 \times 10^{-4}$$
$$\beta = 8.27 \times 10^{-5}$$

Similarly, given that the density of carbon in a multilayer system is around 2.2 g/cm^3, the density of carbon atoms in the carbon layers in the multi-layer mirror is

$$\phi x_C = N_A \ (2.2 \text{ g cm}^{-3}) \ / \ 12.01 \text{ g}$$
$$= 1.10 \times 10^{23} \text{ atoms cm}^{-3}$$

Using the same values of the scattering coefficients, the index of refraction of carbon is obtained:

$$\delta_C = 9.73 \times 10^{-4}$$
$$\beta_C = 1.83 \times 10^{-4}$$

The density of Tungsten in a multilayer system is around 16.3 g cm^{-3} and the atomic weight is 183.85. The values of the scattering coefficient are:

$$f_{1W} = 19.36$$
$$f_{2W} = 22.70$$

which give the index of refraction of tungsten:

$$\delta_W = 9.29 \times 10^{-3}$$
$$\beta_W = 1.09 \times 10^{-2}$$

B: Window Material and its Effects

The ratio T of the transmitted intensity to the incident intensity of light through a layer of substance of thickness t, mass density ρ and mass absorption coefficient μ is

$$T = \exp(-\mu\rho t)$$

Since optimally T is as near unity as possible, the factor $\mu\rho t$ should be as small as possible, so attention should be paid to the values μ of the materials used as windows.

The atomic absorption coefficients μ_A (cm^2/g), where A is the atomic mass, are tabulated. The absorption coefficient of a material which contains n_A atoms of atomic mass A and mass absorption coeffiecient μ_A is

$$\mu = (\sum A\ n_A\ \mu_A)/(\sum A\ n_A)$$

where the summations are over the A values. At the C-Kα line, the values of the atomic absorption coefficients of Hydrogen, Carbon and Oxygen are[3]:

$$\mu_H = 4.62 \times 10^2\ cm^2/g$$
$$\mu_C = 2.35 \times 10^3\ cm^2/g$$
$$\mu_H = 6.04 \times 10^3\ cm^2/g$$

which for Formvar ($C_5H_7O_2$) gives

$$\mu = (7\mu_H A_H + 5\mu_C A_C + 2\mu_O A_O)/(7A_H + 5A_C + 2A_O)$$
$$= 3.41 \times 10^3\ cm^2/g$$

and similarly for Kimfol gives

$$\mu = 2.94 \times 10^3\ cm^2/g$$

Since the densities of Formvar and Kimfol are approximately equal (around 1.0 g cm^{-3}), their factors of $\mu\rho$ are approximately equal, also. Other window materials exist, such as poly-propylene and carbon, and their coefficients of absorption and mass densities are not significantly different from those of Formvar and Kimfol. But Formvar can be made into a film which much thinner than than the sheets of Kimfol, poly-propylene, or carbon, so that its factor of $\mu\rho t$ is much closer to 0 and its transmission factor is much closer to unity. So,

in this work, Formvar windows were used in order to provide maximum flux at the sample.

Window material also acts as a selective filter of the incident radiation; the factor μ, and hence the transmitted intensity, is a function of the wavelength of the incident radiation. Figure 14 shows the calculated value of the mass absorption coefficient of Formvar as a function of radiation wavelength[4]. This figure shows that some of the incident radiation in the lower energy range will be filtered out of the beam through the Formvar, which provides nearly monochromatic C-Kα radiation, and removes radiation from impurities such as oxygen on the anode. However, since the frequency distribution of the incident radiation is small and the Formvar is thin, this effect is not extreme.

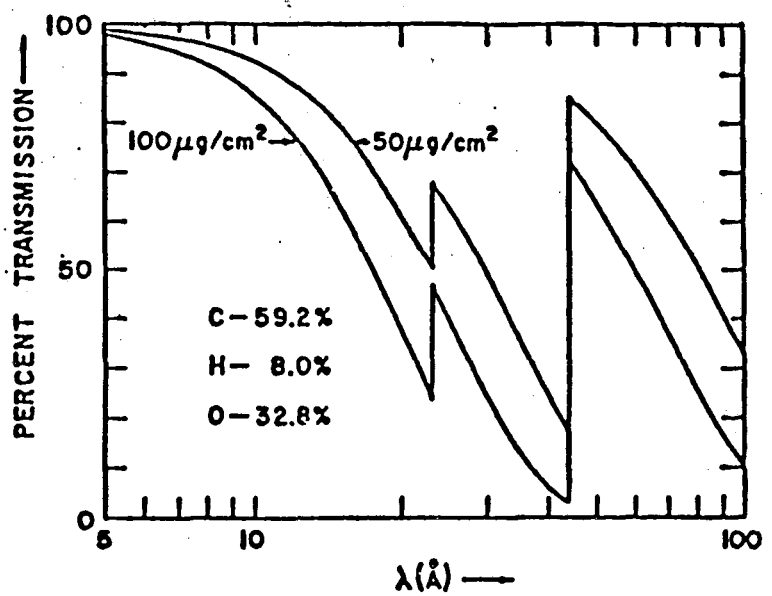

Figure 7: Formvar Transmission vs. Radiation wavelength.

C: Film Characteristics

Several types of film may be used in the x-ray region. Two types of film were used in this experiment: Kodak SB-392 and Kodak 101-07 film. The sensitivities of these films have been reported[7] as a function of the energy of the incident light. For V-Lα radiation, 101-07 film is approximately 10 times more responsive than SB-392. However, it is only about twice as responsive as SB-398 film to C-Kα radiation. 101-07 is difficult to handle because it lacks a protective overcoat of gelatin; merely bending or touching the surface of the unexposed film results in a dark mark in the developed film. In this respect it is preferable to work with SB-392 film, which does not have these limitations. So SB-392 film was used for the C-Kα radiation and 101-07 for V-Lα.

A significant feature of film is that the magnitude of its response does not increase linearly with the exposure time or intensity. The optical density D of an exposed and developed piece of film is defined as

$$D = \log_{10}(1/\tau)$$

where τ is the ratio of the intensity of light transmitted through the film to the intensity of the light incident upon the film. Approximately[6],

$$\log D = A(\log I)^2 + B \log I + C$$

where I is the intensity in photons per unit area incident upon the exposing film and A, B and C are constants. Unless the intensity of exposing light is known it is not possible to predict the time neccessary to increase the exposure darkness by a given amount, although this can be determined experimentally. So that one does not waste time on pointlessly long exposures, it

is important to realize that it is entirely possible to have to increase the exposure time by a factor of 10 in order to increase the exposure darkness by a factor of two.

D: Reflection from a Multi-layer Mirror

An integral component of one of the devices used in this experiment is the periodic multi-layered mirror, which serves as a focussing device of the x-rays.
A multilayer mirror consists of many alternating layers of material with indices of refraction n_1 and n_2, where both indices are very close to unity. For normal incidence, if the optical path of the multilayer structure is equal to $\lambda/2$, the total reflected wave is the constructive interference of many waves reflected from the layer interfaces. Thus it is much more intense than the reflected wave from a single interface.

The tungsten-carbon multilayered mirror with 2d = 44.8 Å was made by magnetron sputtering onto an optically flat curved surface (radius 50 mm) to reflect C-Kα radiation (λ = 44.8 Å) at normal incidence.

E: The Diffracting Samples

The samples we used were polystyrene $[(C_6H_5CHCH_2)_x]$ spheres from Duke Scientific[8]. A broad spectrum of diameters was obtained, but the sizes we used were of diameters

$d = 895nm \pm 8nm$

$d = 597nm \pm 5nm$

$d = 496nm \pm 4nm$

$d = 398nm \pm 4nm$

The quoted specific gravity of the spheres was $1.05\ g\ cm^{-3}$, and they were in an H_2O solution of 10% solids. We also had a bottle of poly methyl methacrylate spheres of diameter 300 - 500 nm, which were used primarily in the pinhole collimation device.

To support the spheres we used Kimfol $(C_{16}H_{14}O_3)$ in the pinhole collimation device, and Formvar $(C_5H_7O_2)$ in both devices. We used vacuum grease as an adhesive between the Kimfol/Formvar and the window frame.

To distribute the spheres onto the window, several methods were tried. First we simply dropped the spheres in the original solution onto the Kimfol, but no wetting took place so that the sphere-solution did not distribute itself onto the Kimfol but held itself in a drop formation. If the spheres were dropped onto a drop of photo-flow or distilled water which was already on the formvar, they could be distributed. After a single coat of spheres was on the window, subsequent coats did not require a wetting agent to facilitate spreading. When using the pinhole-diffraction device, we varied the number of coats of spheres to achieve samples of varying thickness. When using Formvar, we again dropped distilled water onto the window before dropping the sphere solution into the water, and used a tilting action and occasionally a cotton swab to spread the solution about the Formvar. The Formvar is much thinner than the

Kimfol, so that it wrinkled from the water placed over it. This allows the spheres to clump into the wrinkles, and combined with the long drying time of the water, allows ordered arrays to form on the Formvar. The last method used was to place the spheres in alcohol and place some drops of this solution onto the Formvar. Alcohol reduces the surface tension of the sphere solution and dries quickly to reduce probability of packing; it also dissolves Formvar. We found that a sample could be made by placing a drop of the alcohol solution onto the Formvar, tilting the Formvar film, and allowing the alcohol solution to diffuse across the Formvar. The Formvar was unable to wrinkle as it was in a semi-fluid state, so clumping was minimized. Thicker samples are made by successive applications of the sphere-alcohol solution.

Figures 8(a) and 8(b) are electron micrographs of low and high magnifications, respectively, of samples which were made using an aqueous solution of 597nm diameter spheres on Formvar. They show very distinct hexagonal lattice patterns. As explained in the theory section, these samples will produce sharp diffraction patterns, which are smaller than the patterns expected from a single sphere of the same radius. Figures 9(a) and 9(b) are such pictures for a single application of an alcohol solution of 597nm diameter spheres on Formvar. They show that while there is clumping of spheres, there is no ordered pattern in the sample. Again, these samples will produce diffuse diffraction patterns which are approximately equivalent to the diffraction pattern from a single sphere. As stated earlier, since in most experiments one expects a scattering pattern of a single sphere, these are the samples which are of primary interest in this work.

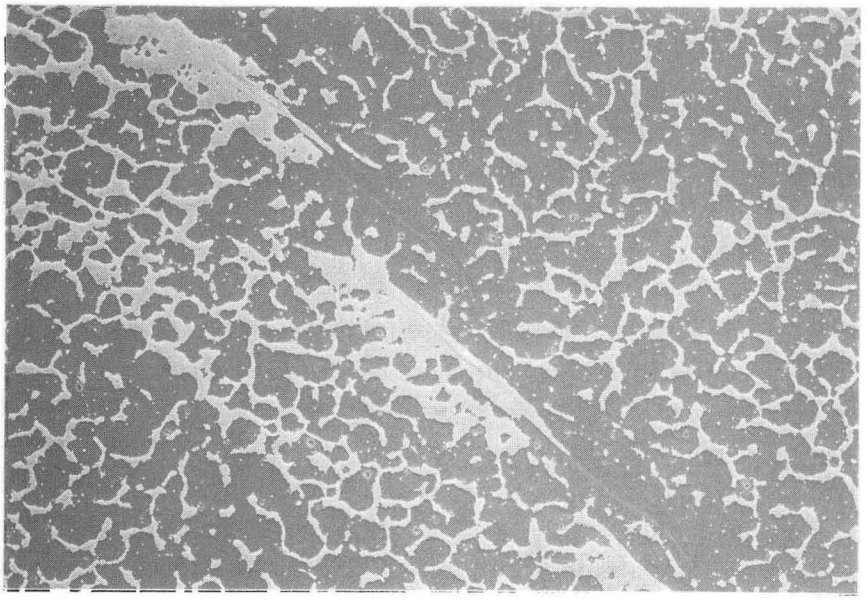

100U

XBB 884-3025

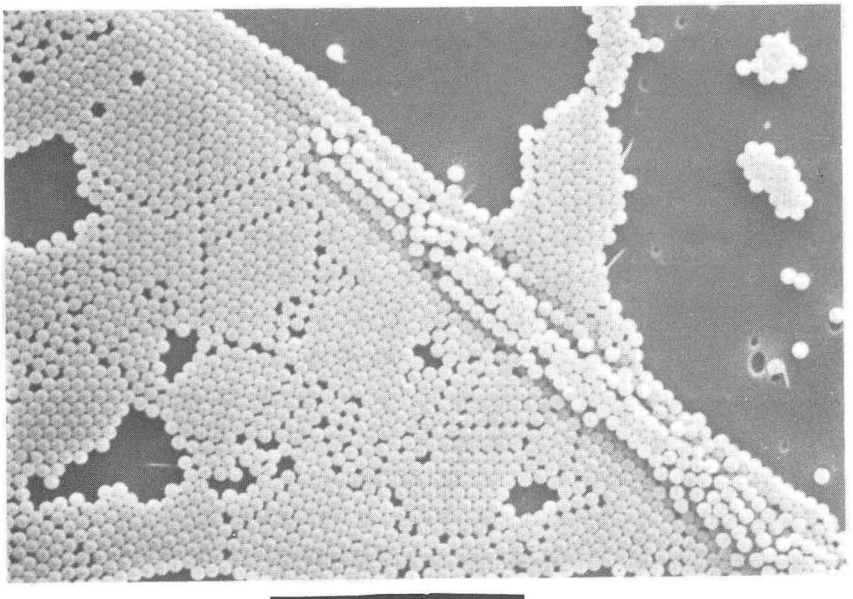

10U

XBB 884-3029

Figures 8(a),(b): Scanning electron micrographs of 597 nm diameter spheres from a H_2O solution.

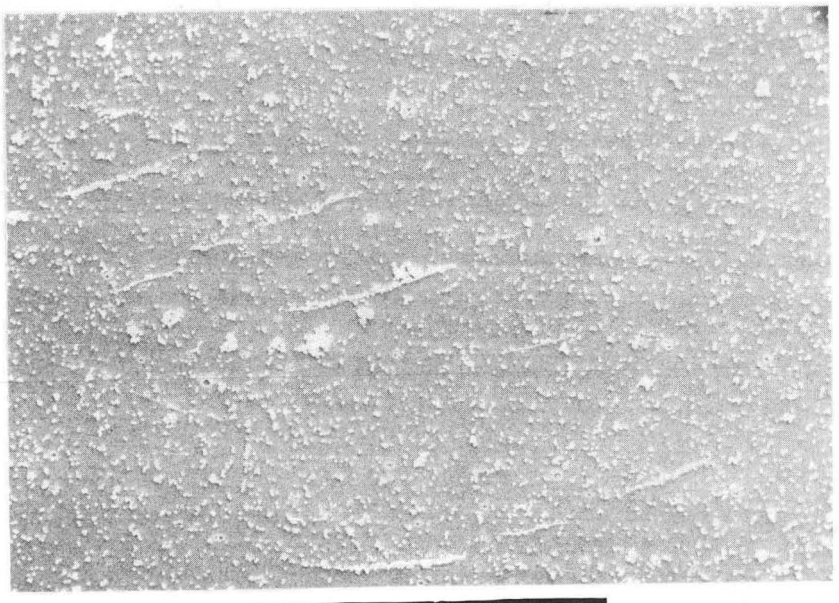

100U

XBB 884-3026

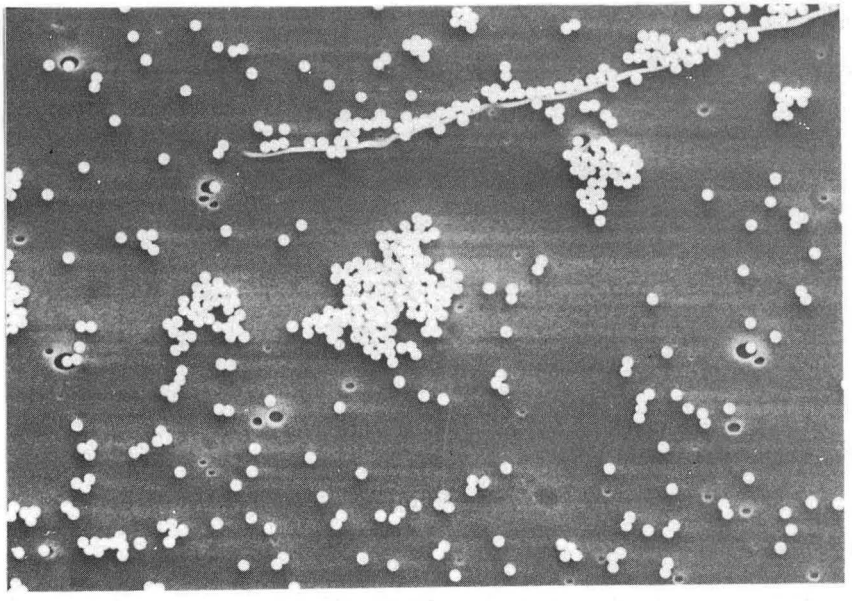

10U

XBB 884-3031

Figures 9(a),(b): Scanning electron micrographs of 597 nm diameter spheres from an alcohol solution.

F: The X-Ray Source

Figure 10 is a schematic of the simple conventional x-ray source which we used in this experiment. As shown in the figure, electrons are ejected from the filament, which is at a relatively low voltage. They are focussed by the walls of the system, which are also at a relatively low voltage, onto the anode, which is at a relatively high voltage.

The current through the filament was set at 20 mA. In order to verify that the radiation produced was C-Kα (or V-Lα) a diffraction grating was inserted over the top pinhole of the pinhole diffraction device (later section) and a short exposure was taken. The first maxima observed showed that C-Kα radiation was definitely obtained. When using a vanadium anode, however, it was found that the anode must be well cleaned of surface impurities arising from the vacuum system, in order to produce strong V-Lα radiation. Otherwise a strong source of C-Kα radiation was present.

Figure 11 is a photograph of the lower section of device used in this work. On top is the source diagrammed in Figure 10. On bottom are a tuning micrometer and the leads to the water cooling circuit. This section is held in the bottom of a (coaxial) cylinder. Figure 12 is a top view of this arrangement, showing the open cylinder, another section of the water cooling circuit, and the top of the anode in the lower center. The devices which were used in this work were connected to the cylinder via a large flange (plexi-glass or aluminum) which was bolted onto the top section of this cylinder. The entire system was kept under a vacuum of around 10^{-6} torr.

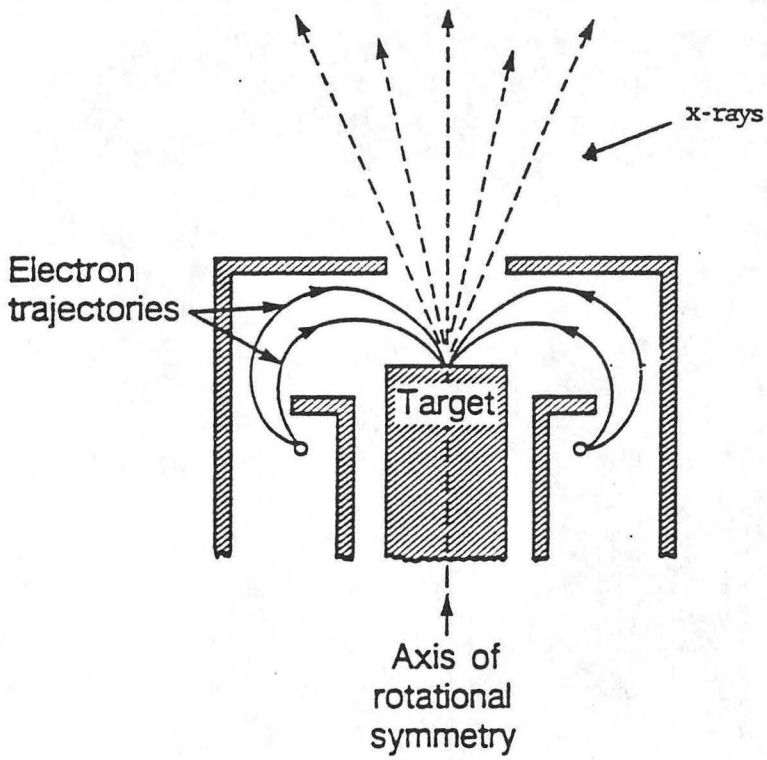

Courtesy of Ralph Feder, IBM

Figure 10: The simple conventional x-ray source.

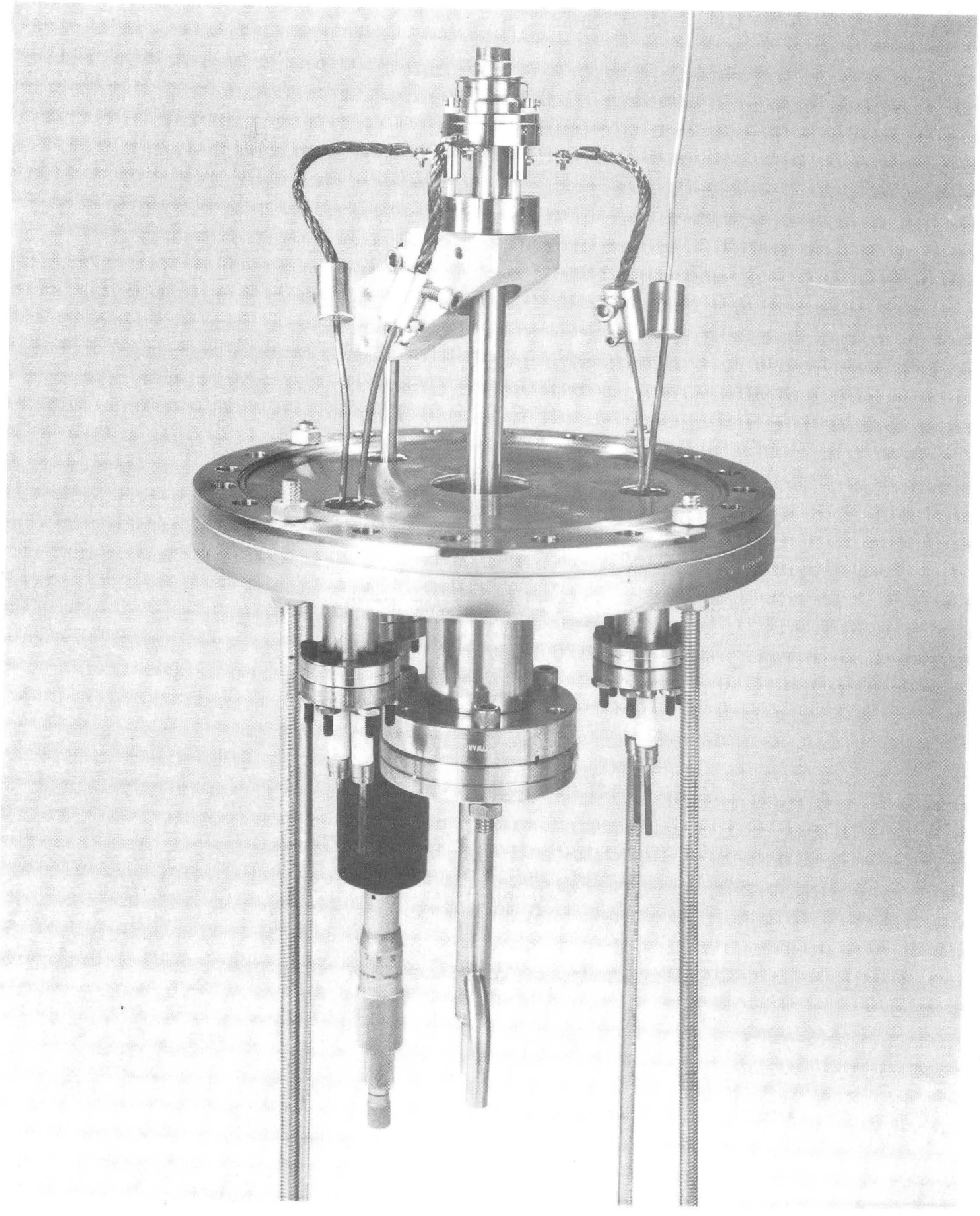

Figure 11: The lower section of the x-ray source.

CBB 868-6659

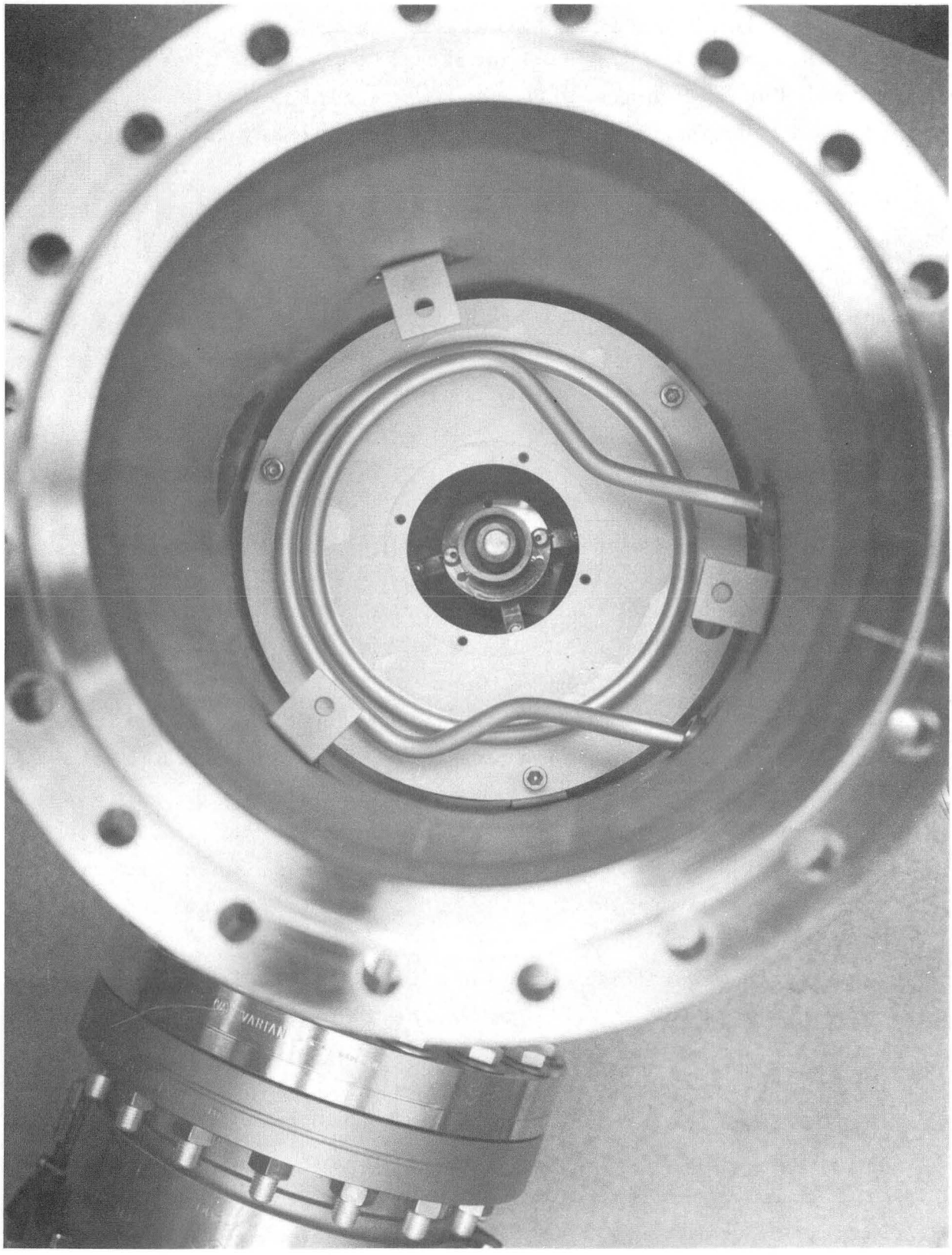

CBB 867-5741

Figure 12: Top view of the x-ray source while inside the coaxial cylinder.

G: The Pinhole Collimation Device

Figure 13 is a schematic of the first device we used. Under Pinhole 2 is the Latex disk which was bolted to the top of the cylinder of the x-ray source (see section B). Two pinholes of diameters 13/1000 inch, located above the source, collimate the x-rays. With no diffracting sample in its path, radiation from the second pinhole will image the first pinhole onto the film, which is mounted 50 cm from the second pinhole. The size of this spot may be determined by geometrical optics, since the ratio of the pinhole diameters to the radiation wavelength (7×10^4) is much greater than unity. By using simple ray-tracing techniques and the known diameters (0.033 cm) and spacing (19 cm) of the pinholes, the maximum axial angle of the undiffracted light is

$$\theta_{max} = (0.033 \text{ cm})/(19\text{cm}) = 1.7 \times 10^{-3} \text{ radians}$$

so the diameter of the image of the first pinhole through the second pinhole is

$$d = 2\ \theta_{max}(50 \text{ cm}) = 0.17 \text{ cm}$$

These values are approximate, since there is significant uncertainty in the diameters of the pinholes, but they allow an estimate of how large a diffraction pattern must be in order to be observed; the angle of the diffracted light must be at least 1.7×10^{-3} radians, which is true for the secondary maxima of diffraction patterns of C-Kα radiation from sub-micron diameter spheres. Also, the spot size of undiffracted light shows how focussed the diffraction pattern will be. The centers of diffraction patterns of radiation incident in different directions will be distributed about the spot area; if the image of the first pinhole is very small, the diffraction pattern from the sample will be very focussed. The inverse is also true. However, even if the spot area is relatively large, if the radius of the first secondary maximum is much greater than the radius of the spot size (as it is

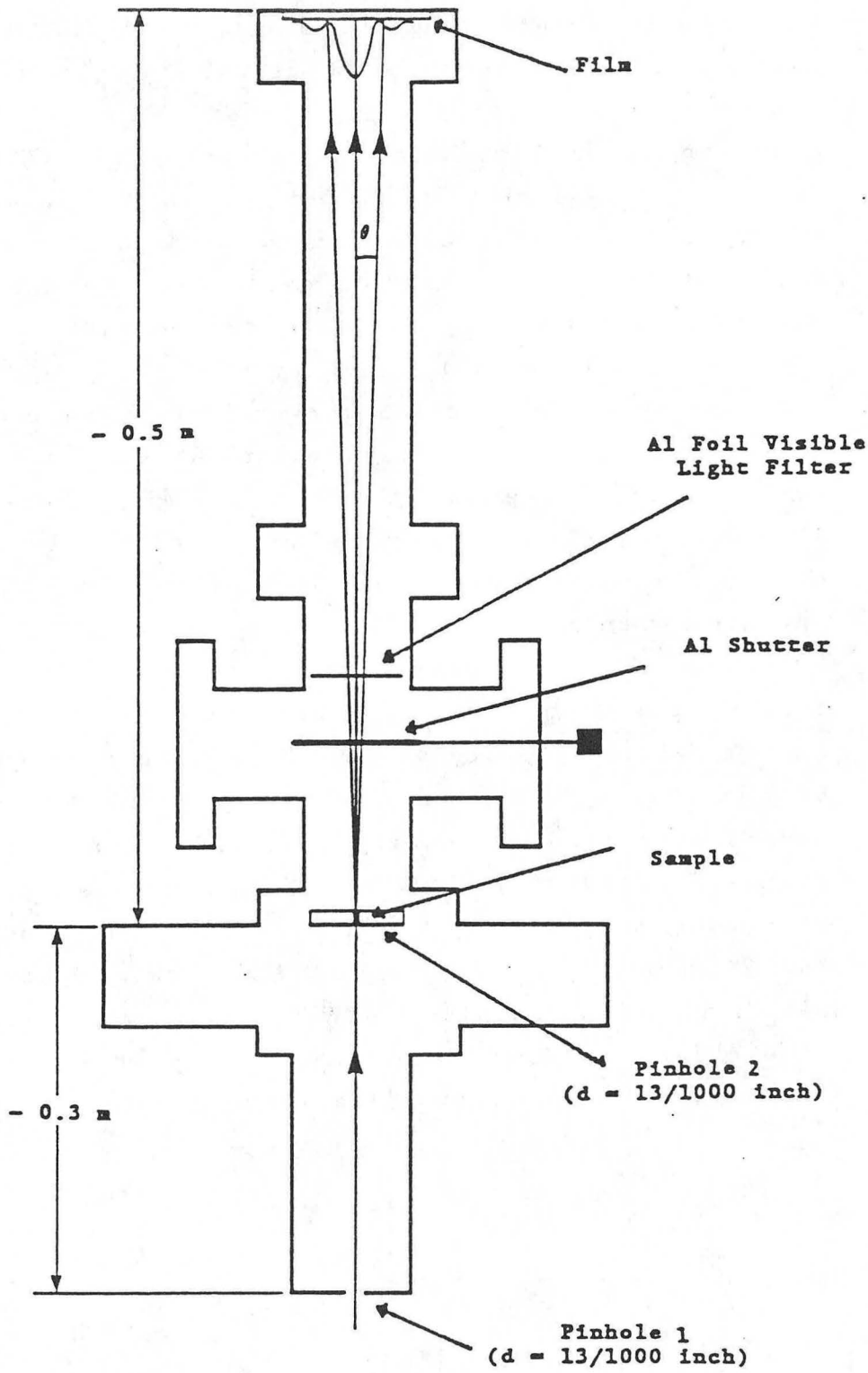

Figure 13: The pinhole collimation device.

for this device), the locations of secondary maxima of any pattern should roughly coincide and the diffraction pattern will be reasonably focussed.

A sample of spheres is mounted a few millimeters above the second pinhole on a rectangular piece with a large circular aperture, resting on the allen screws which hold the pinhole assembly to the central flange. Any scattering of light is detectable if the light is scattered sufficiently far from the unscattered path and if it is of sufficient intensity.

As explained in the theory section, the intensity of scattered light when using the pinhole collimation device is severely limited by the area of the sample which is illuminated. That this area is the relatively small area of the pinhole explains the lack of observed diffraction patterns when using this device. We used C-Kα (44.8 Å) and V-Lα (24.3 Å) radiation, and samples of thickness ranging from approximately a single layer of spheres to an entirely opaque (to visible light) coat of spheres, on both Kimfol and Formvar. Exposure times of up to 24 hours were tried, resulting only in diffraction from the pinhole. Figure 14 shows the film from an exposure with an opaque sample and C-Kα radiation. The exposure time was 24 hours. Figure 15 is film from another exposure with an opaque sample and V-Lα radiation, of exposure time 4 hours. This figure incidently shows the size of the pinhole image at the film (around 2mm in diameter).

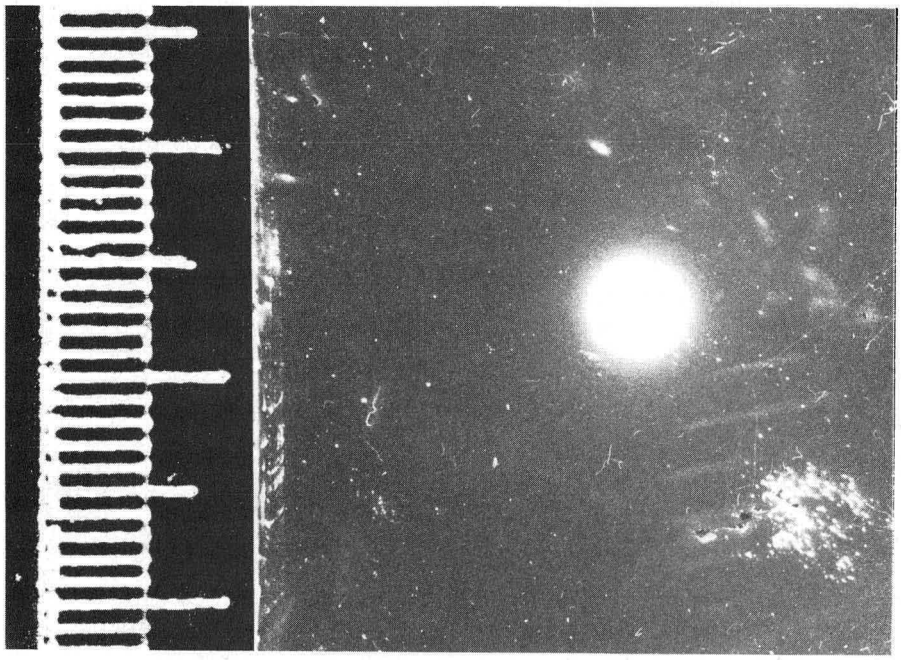

XBB 893-1564

Figure 14: Resulting intensity distribution from a 24 hour exposure using C-Kα radiation.

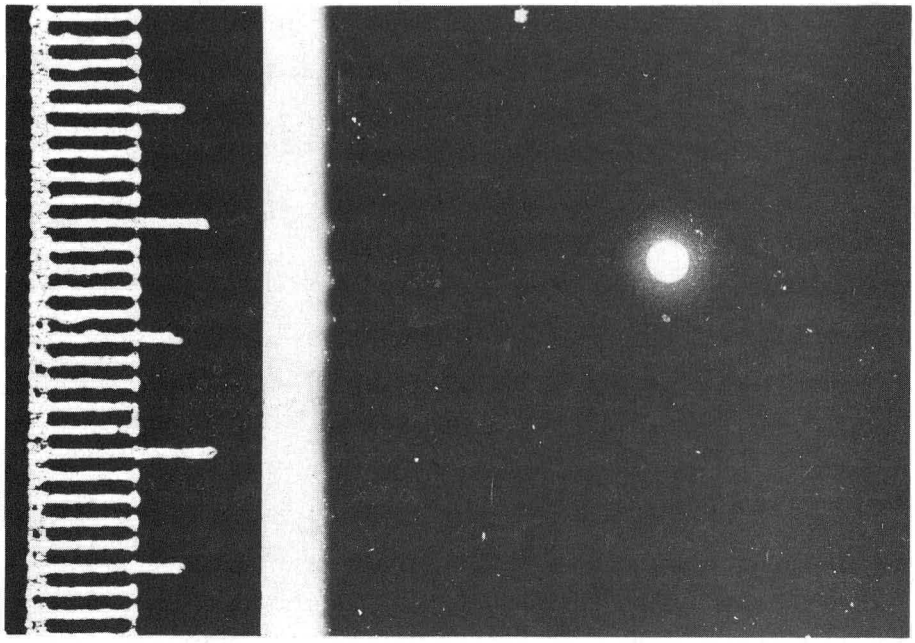

XBB 893-1565

Figure 15: Resulting intensity distrubution from a four hour exposure using V-Kα radiation.

H: The Multi-layer Mirror Device

Figure 16 is a schematic of the second device we used, and Figure 17 is a photograph of the actual device. Again, the large disk at the center of the device, shown in both figures, connects to the top of the cylinder of the x-ray source. Figures 18 and 19 show the lower flanges of the device, which include the pinhole and the visible light filter. The film is taped onto the side not shown in Figures 18 or 19 of the anodized lower flange. A hole is punched in the film so that the radiation passes through the hole and not the film; the hole eliminates not only attenuation of the radiation by the film but also saturation of the film by the source. Figure 20 shows the upper flange, which contains the mirror and the sample. Figure 21 shows the upper flange and the related components: the sample, the mirror and the ring which holds the mirror inside the cavity of the flange. Incidentally, the colors which appear on the sample assembly are from constructive interference of visible light from the Formvar thin film.

The T-section, the upper cylinder and upper flange of the device are made of stainless steel, while the middle and lower flange, the lower cylinder, the shutter and the ring which secures the mirror to the upper flange are made of aluminum. To avoid fogging of the film[9] due to the "Russel Effect", the lower aluminum components of the device were anodized.

Again the diameter of the pinhole shown in Figure 16 is 13/1000 inch, but the light from the (extended) source is not collimated, so that the image of the source on the mirror is determined primarily by the size of the source rather than diffraction. At any rate, the area of the mirror illuminated is much greater than the area of the pinhole--if the distance of the pinhole from the source is 30 cm and the source is 5mm in diameter, the image of

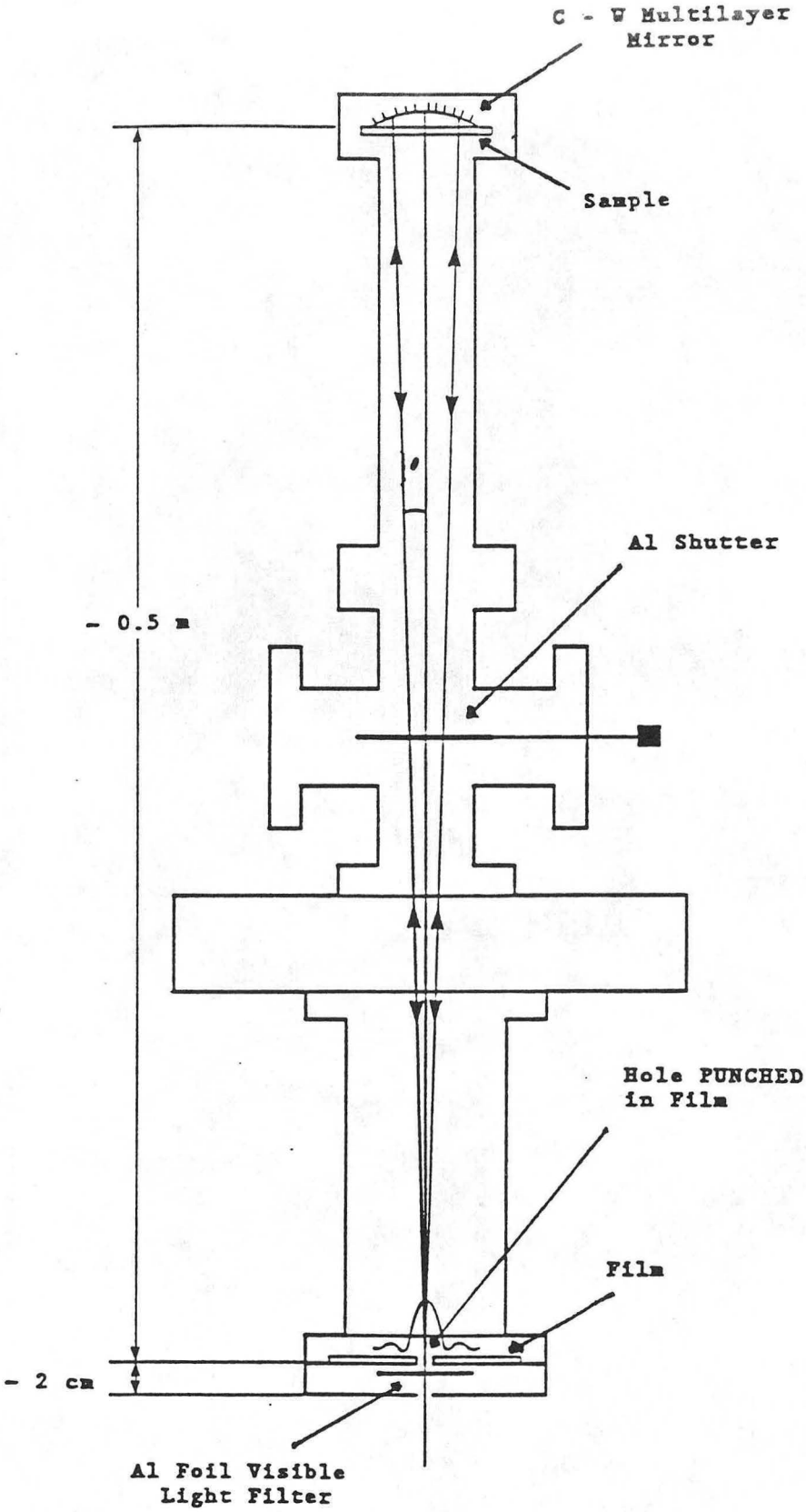

Figure 16: The multilayer mirror device.

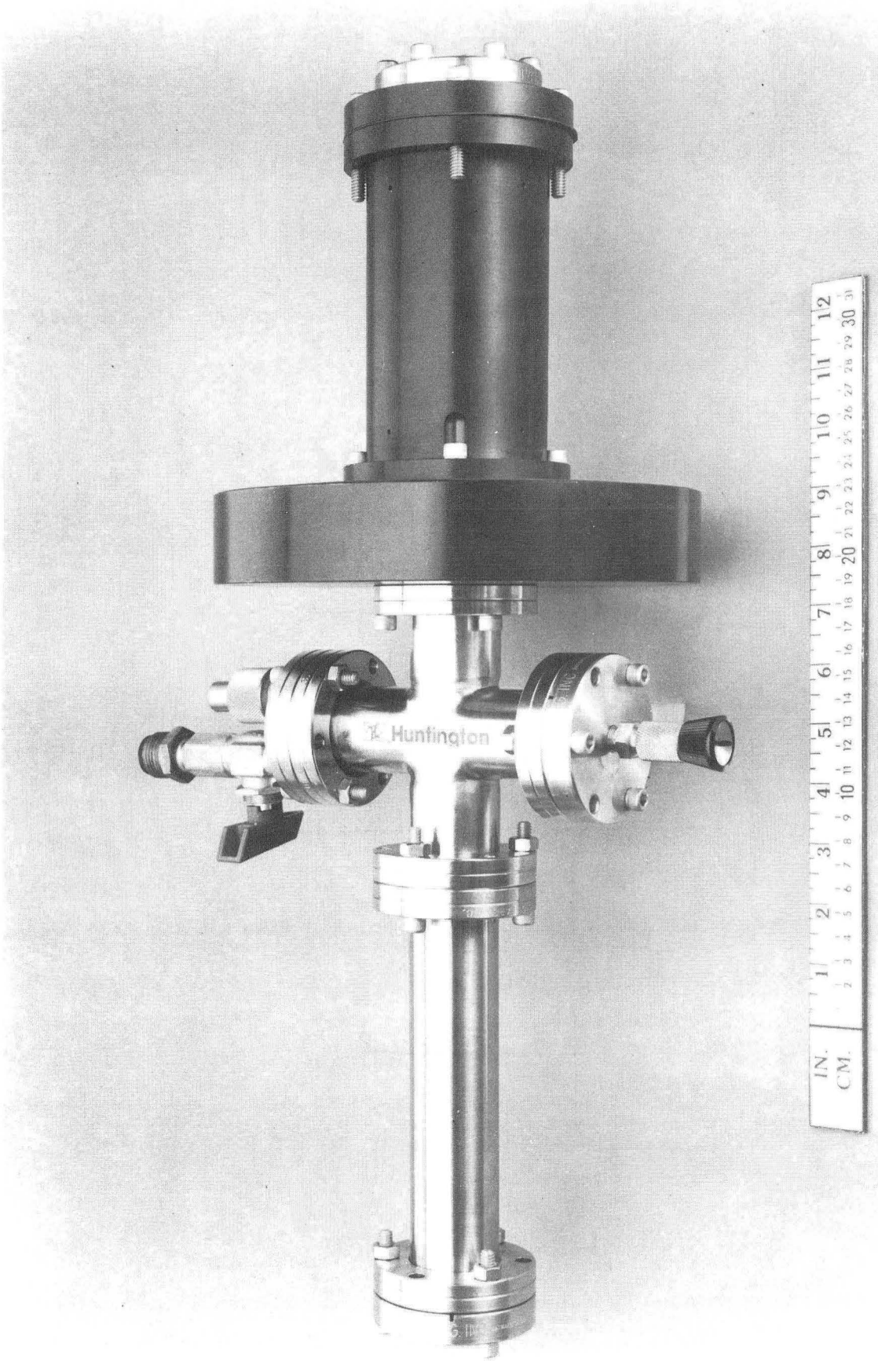

CBB 884-4106

Figure 17: The multilayer mirror device.

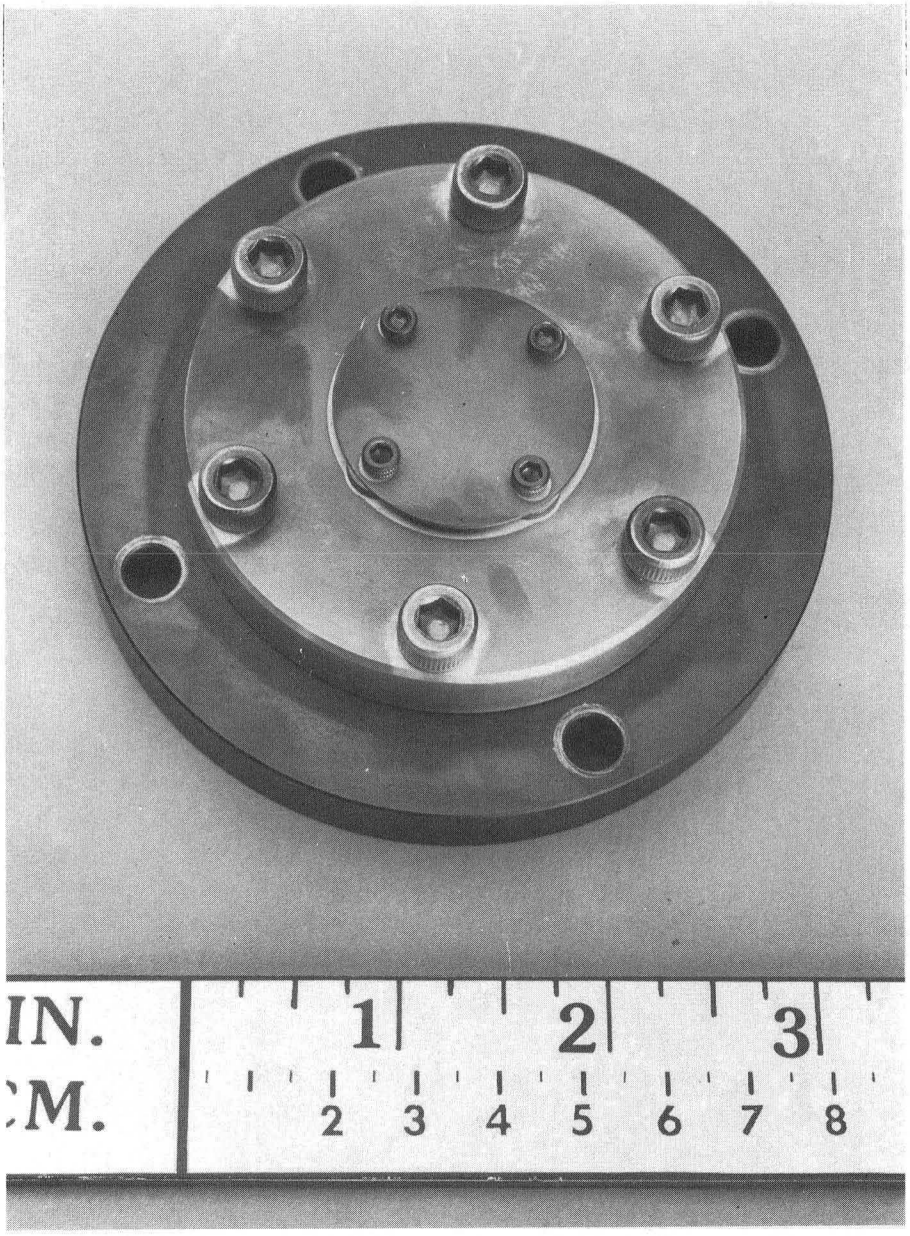

CBB 884-4112

Figure 18: The lower flange

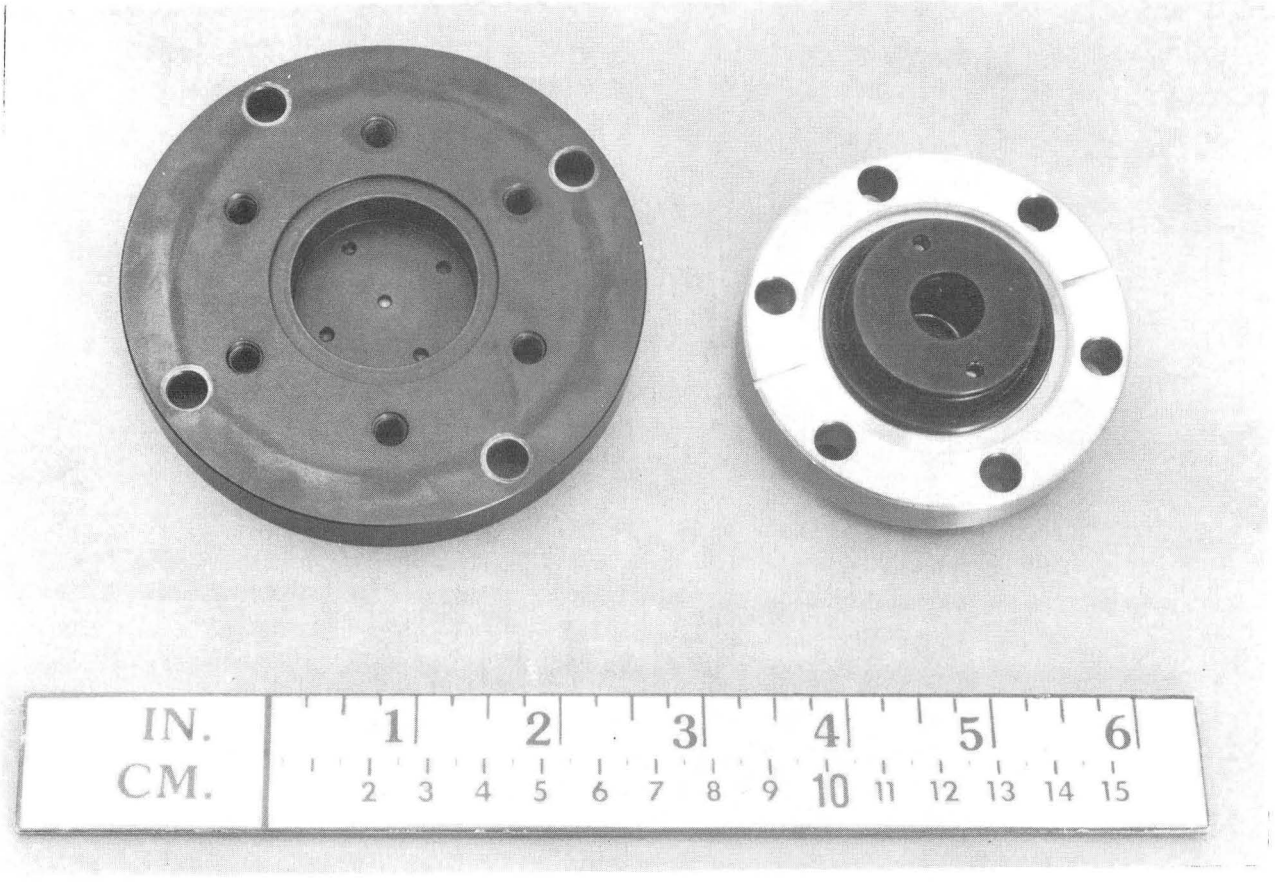

CBB 884-4108

Figure 19: The lower flange, separated. The small black piece holds the visible light filter.

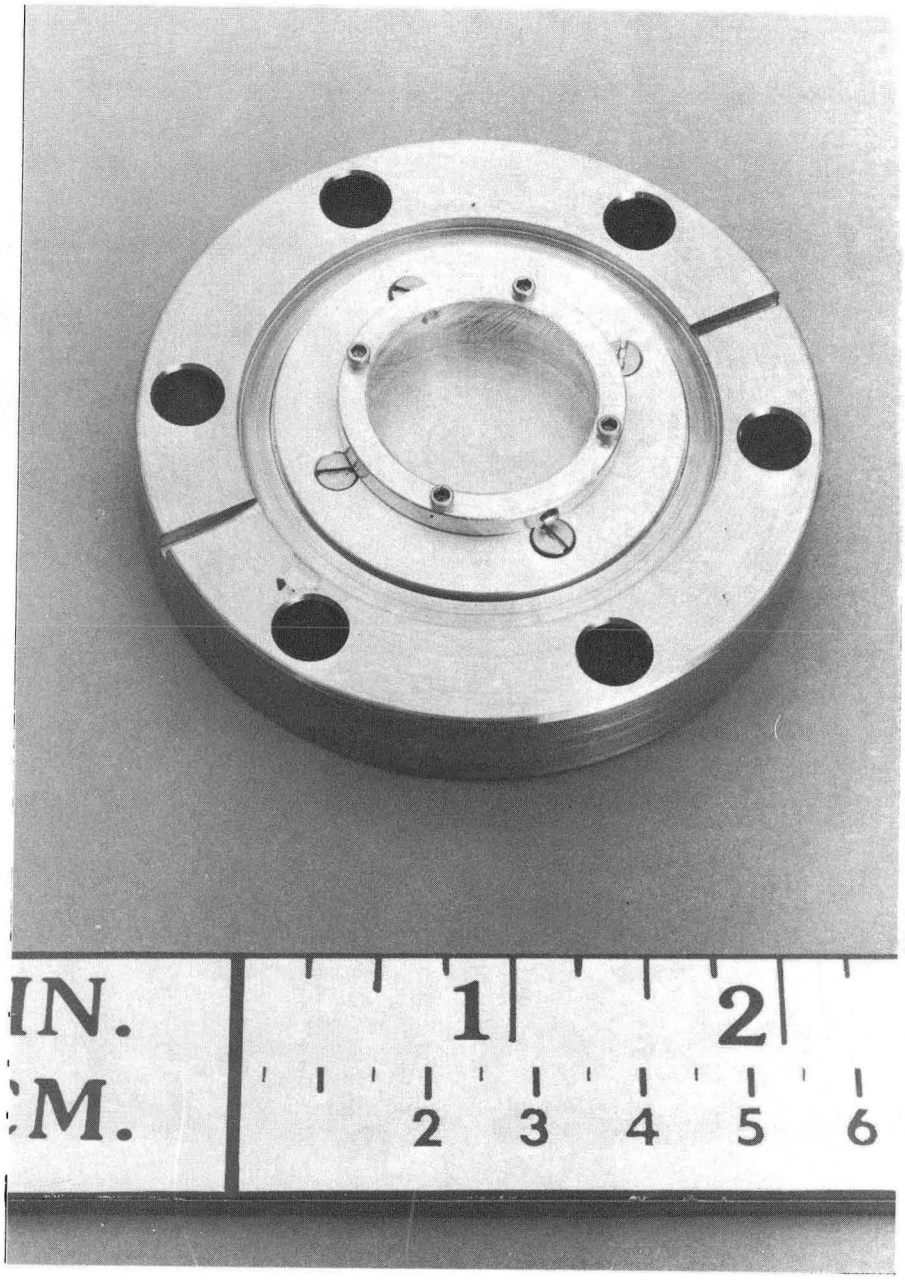

CBB 884-4112 A

Figure 20: The upper flange.

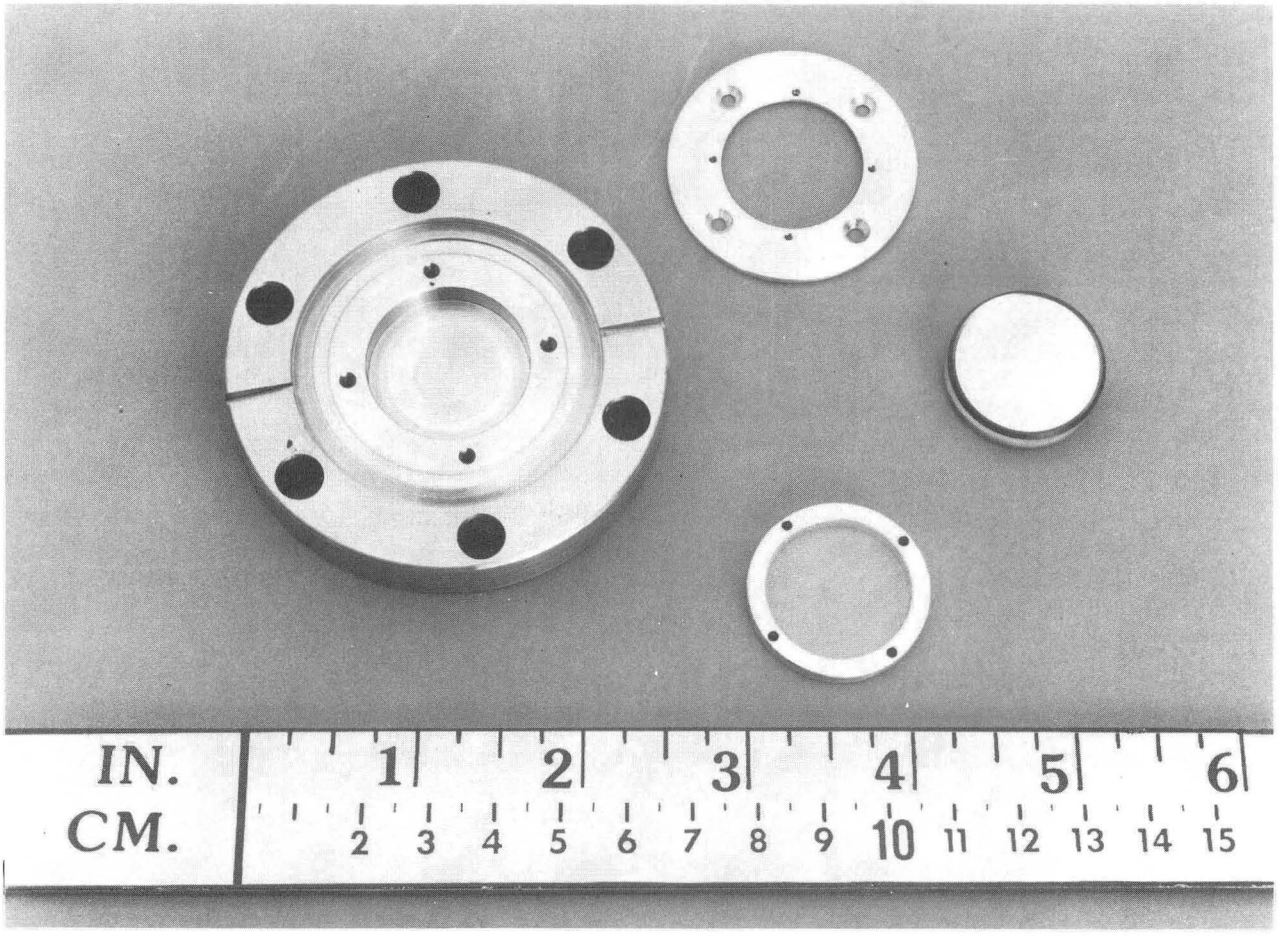

CBB 884-4110

Figure 21: The upper flange and its components: the sample, the mirror and the mirror ring.

the source at the sample will be of diameter

$$d = 2(48\ \text{cm})(0.5\ \text{cm})/(30\ \text{cm}) = 1.6\ \text{cm}\ ,$$

compared to the diameter of the illuminated area of the sample in the pinhole collimation device, 0.033 cm. Thus the effective sample area increases by a factor of around 2000 when the multi-layer mirror device is used instead of the pinhole collimation device.

The radius of curvature of the mirror is 50 cm. Accordingly the pinhole is ~ 52 cm from the mirror, and the film is ~ 48 cm from the mirror. If no sample is present the light from the pinhole is focussed onto the film as a point whose size is determined by the diameter of the pinhole and the distances from the mirror to the film, and the mirror to the pinhole. Since the size of the pinhole is again much greater than the radiation wavelength, diffraction effects are negligible, and the diameter d of the focussed pinhole image on the film is

$$d = (0.033\ \text{cm})(48\ \text{cm})/(52\ \text{cm}) = 0.030\ \text{cm}$$

Light which is scattered at an angle θ will make an image a distance

$$r = (48\ \text{cm})\ \theta$$

from the central focussed spot on the film.

The location of the focal point is slightly off center (that is, it does not coincide with the hole in the film and the pinhole), so that the center of the pattern will not be lost in the punched hole. The sample is mounted on a narrow ring which is mounted onto the mirror assembly. As in the previous device, any diffracted light is detectable if it is scattered reasonably far from the unscattered path. However, since in this geometry many more spheres are illuminated than before, the scattered intensity is much greater than in the previous set-up so that observing a pattern after a reasonable time (about five hours) is much more likely than before.

The calculated relative intensities of diffracted C-Kα radiation from a lattice of 597 nm diameter spheres, whose corner sphere has indices 7 and 9 (notation discussed in theory section), for the azimuthal angles $\phi = 0$ and $\phi = \pi/6$, are presented in Figures 22 and 23, respectively. These figures give the radii of the first and second secondary maxima and it is seen that the angular shift of the maxima of a pure lattice is barely noticeable when the lattice intensity is modulated by the single particle intensity. The first maxima occurs at θ slightly less than $\lambda/(3^{1/2}a)$, and the second at θ slightly less than λ/a. It is thus sufficient to use the formulas $\theta = \lambda/(3^{1/2}a)$ and $\theta = \lambda/a$ for the positions of the first and second maxima.

Several samples made with H_2O-sphere solutions (that is, samples which consist primarily of lattice structures of spheres) were exposed with C-Kα radiation, and diffraction patterns were observed. Reproductions of the photographic plates are presented in Figures 24 and 25. The large divisions of the scales are centimeters. Table 1 presents the locations of the first and second maxima, and the corresponding calculated values.

Again using C-Kα radiation, diffraction patterns from samples which were made from an alcohol-sphere solution were obtained. Figures 26 - 29 are plots of the calculated relative intensities of diffracted C-Kα radiation from spheres of radii 398 nm, 496 nm, 597 nm, and 895 nm, respectively, as a function of axial angle θ. Reproductions of the exposures are presented in Figures 30 - 32. Again, the large divisions of the scales are centimeters. Absent from these reproductions is the exposure made with 496 nm diameter spheres, as the first secondary maxima was too faint to reproduce. Table 2 presents the measured locations of the first secondary maxima, and the corresponding calculated values. The

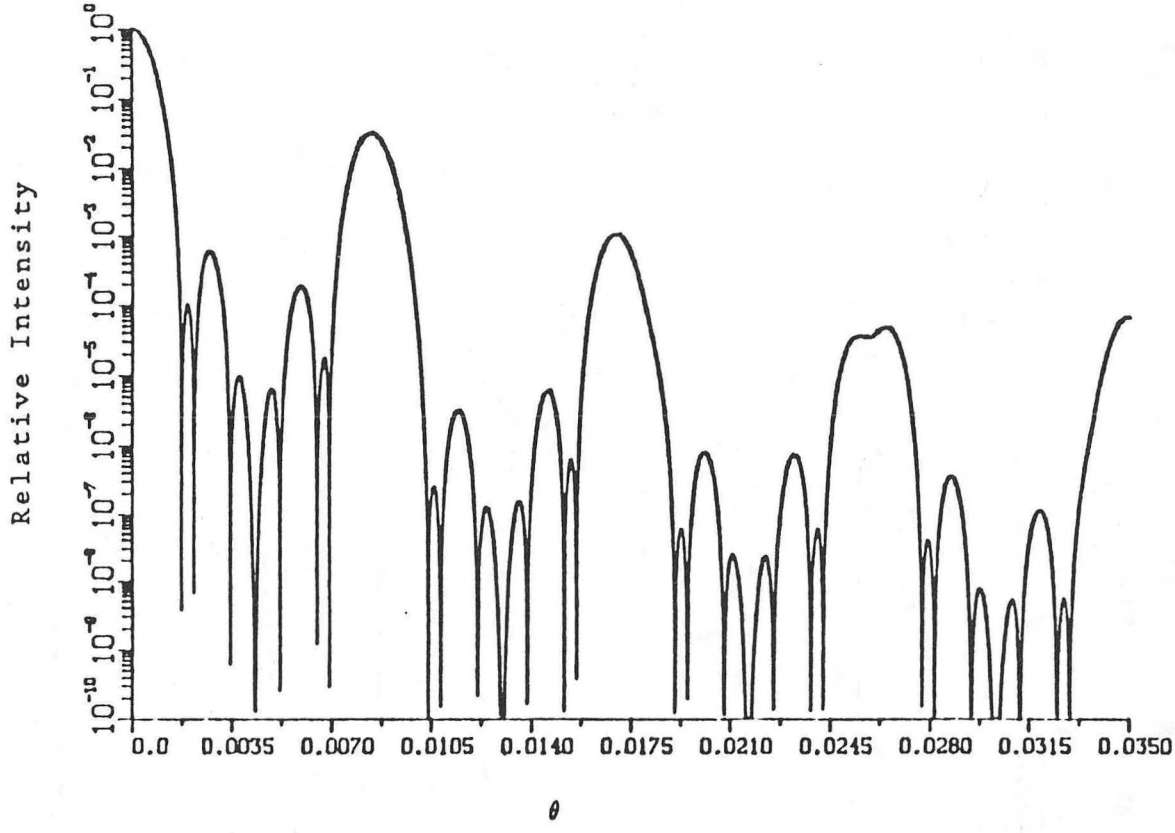

Figure 22: Calculated intensity distribution vs. axial angle ϑ for a close-packed array with dimensions 7x9 of 597nm diameter spheres and radiation wavelength λ = 44.8Å at azimuthal angle $\phi = \pi/6$ (line spacing $d = \sqrt{3}a$).

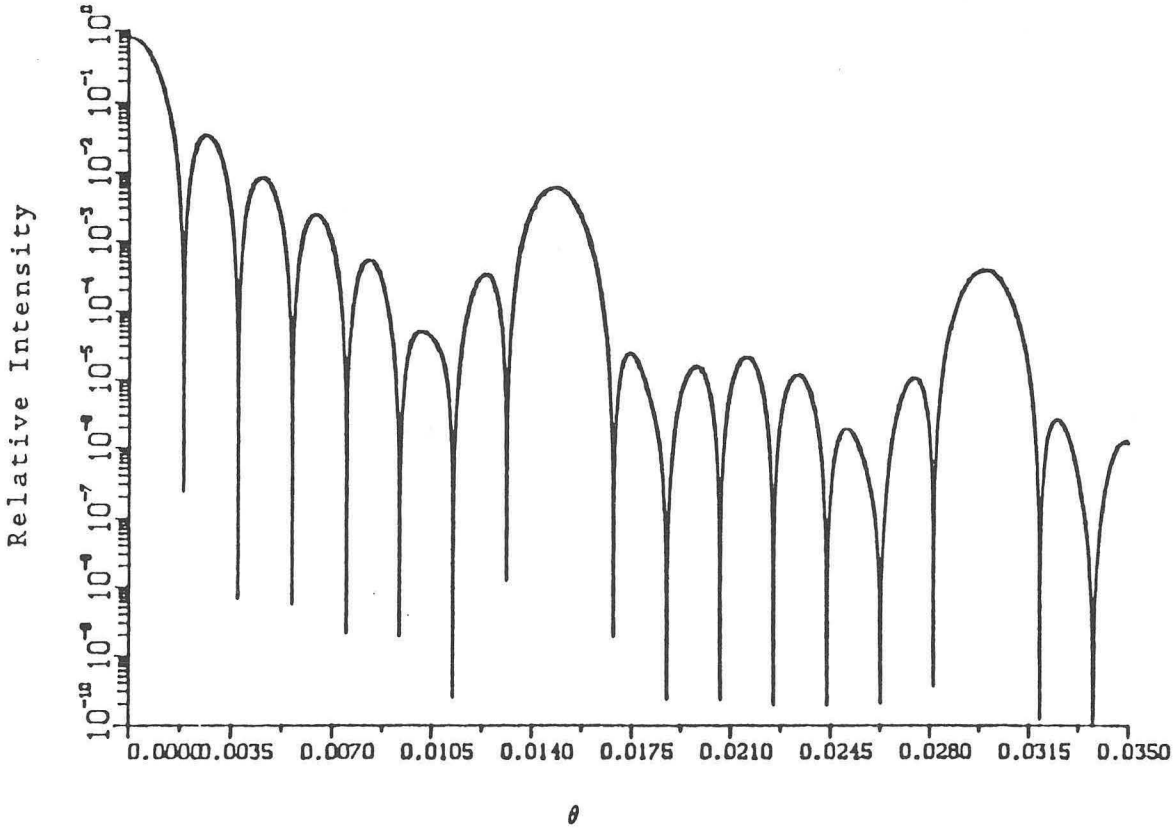

Figure 23: Calculated intensity distribution vs. axial angle ϑ for a close-packed array with dimensions 7x9 of 597nm diameter spheres and radiation wavelength λ = 44.8Å at azimuthal angle ϕ = 0 (line spacing d = a).

uncertainty in each of the measurements is around 0.1 cm.

Both the calculated and observed scattering patterns show that radiation scattered by a lattice structure of spheres forms a pattern which is significantly smaller and sharper than that scattered by an unordered array of identical spheres. In analyzing experimental data one should be aware that sharp diffraction patterns arise from lattice structures, since confusing such diffraction patterns with the larger patterns arising from random arrays of particles will lead to the determination of the incorrect particle size.

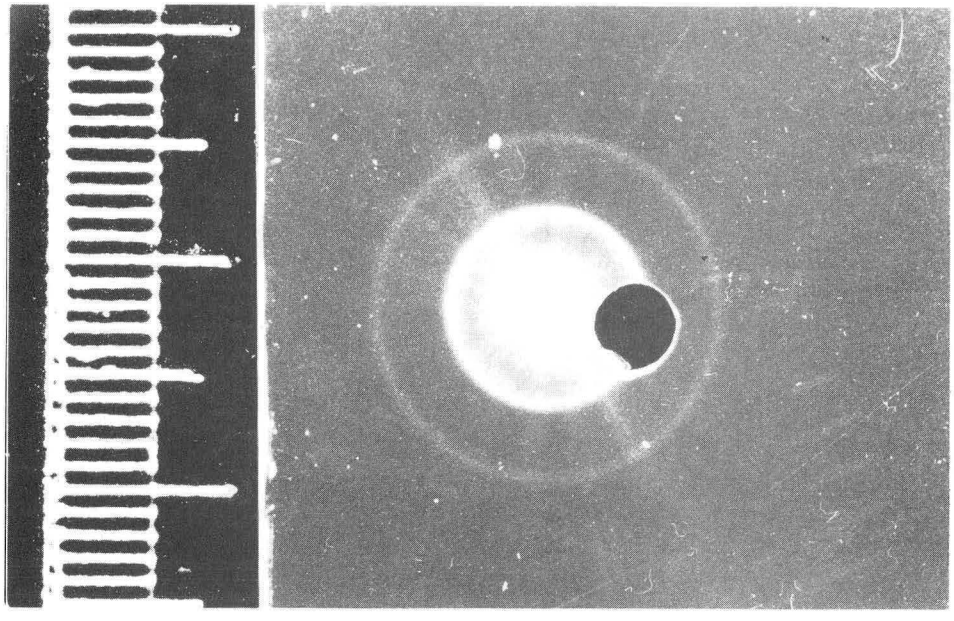

XBB 893-1566

Figure 24: Resulting intensity distribution from a 2.5 hour exposure with C-K radiation and 597nm diameter spheres.

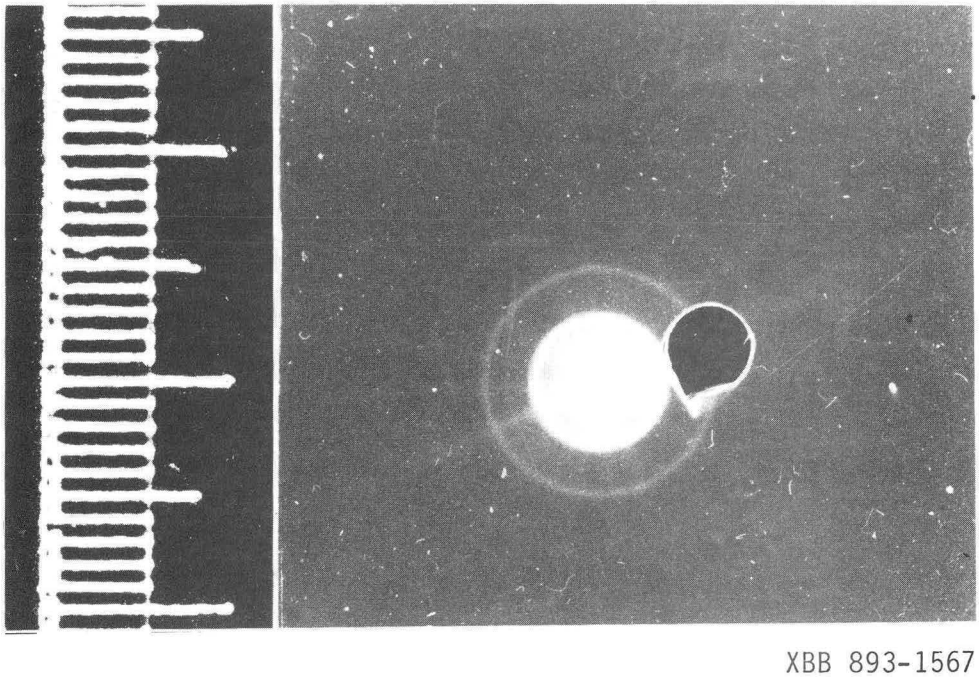

XBB 893-1567

Figure 25: Resulting intensity distribution from a 2.5 hour exposure with C-K radiation and 895nm diameter spheres.

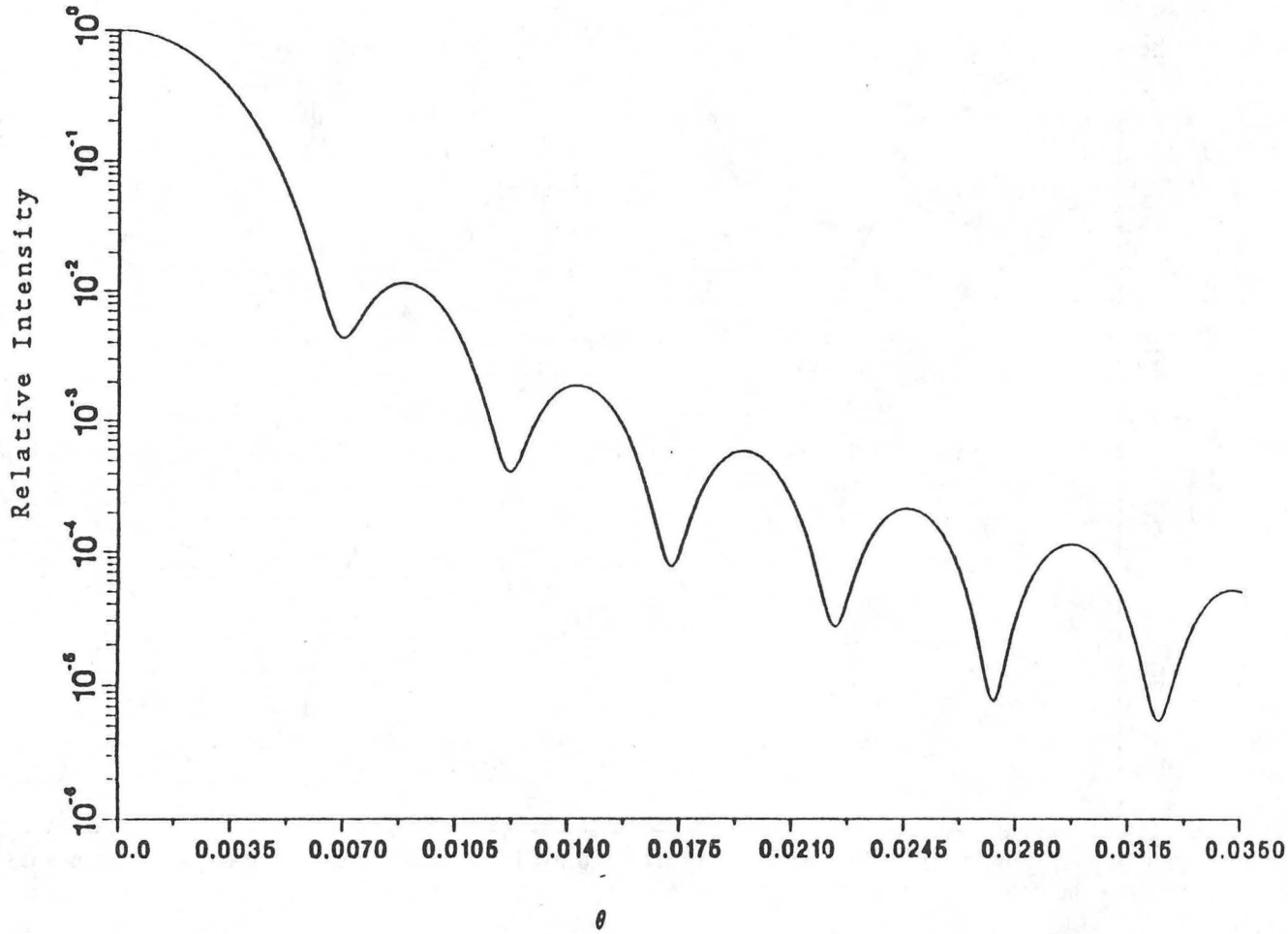

Figure 26: Calculated intensity distribution vs. axial angle ϑ for an unordered array of spheres of 895nm diameter.

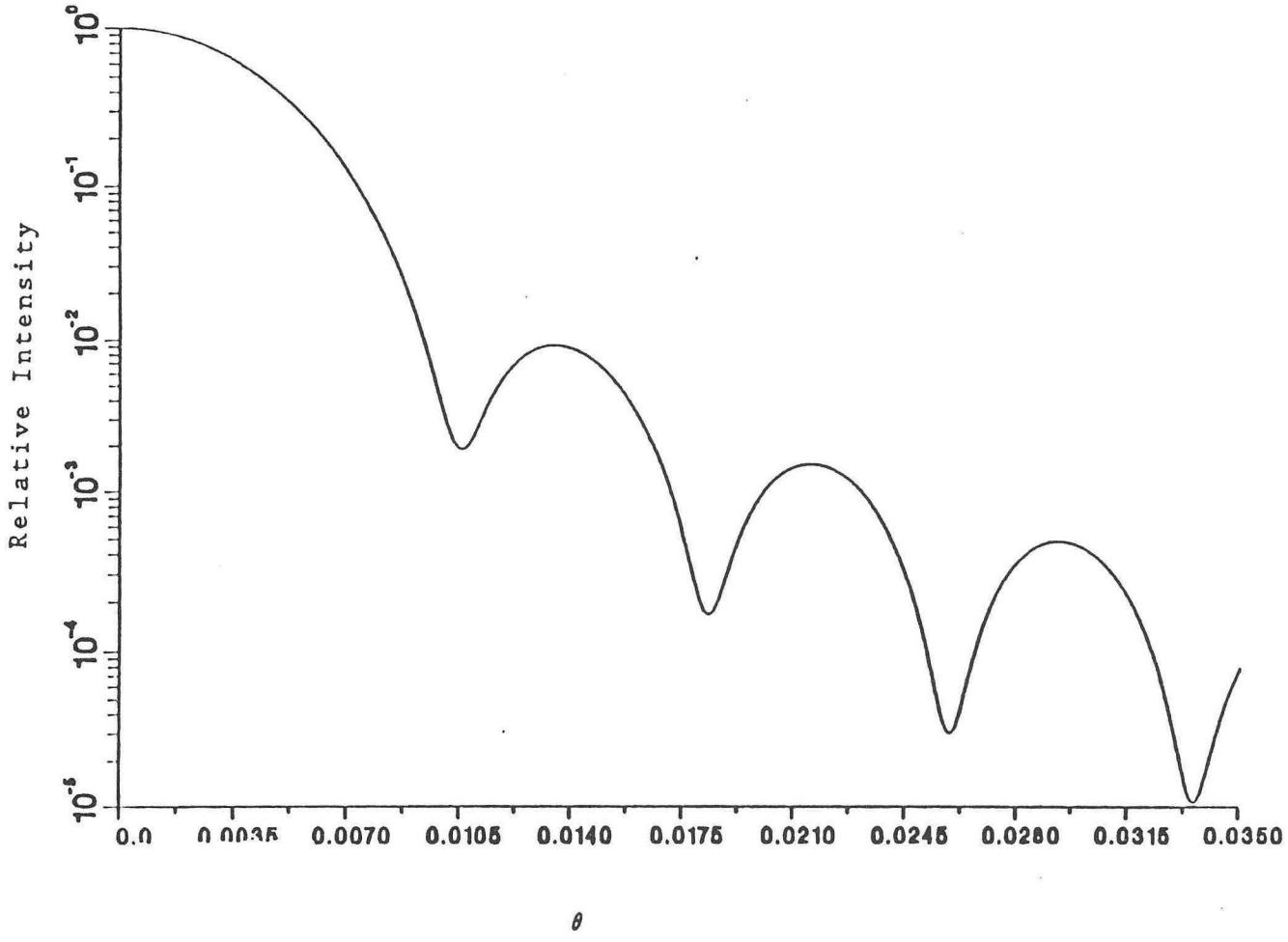

Figure 27: Calculated intensity distribution vs. axial angle ϑ for an unordered array of spheres of 597nm diameter.

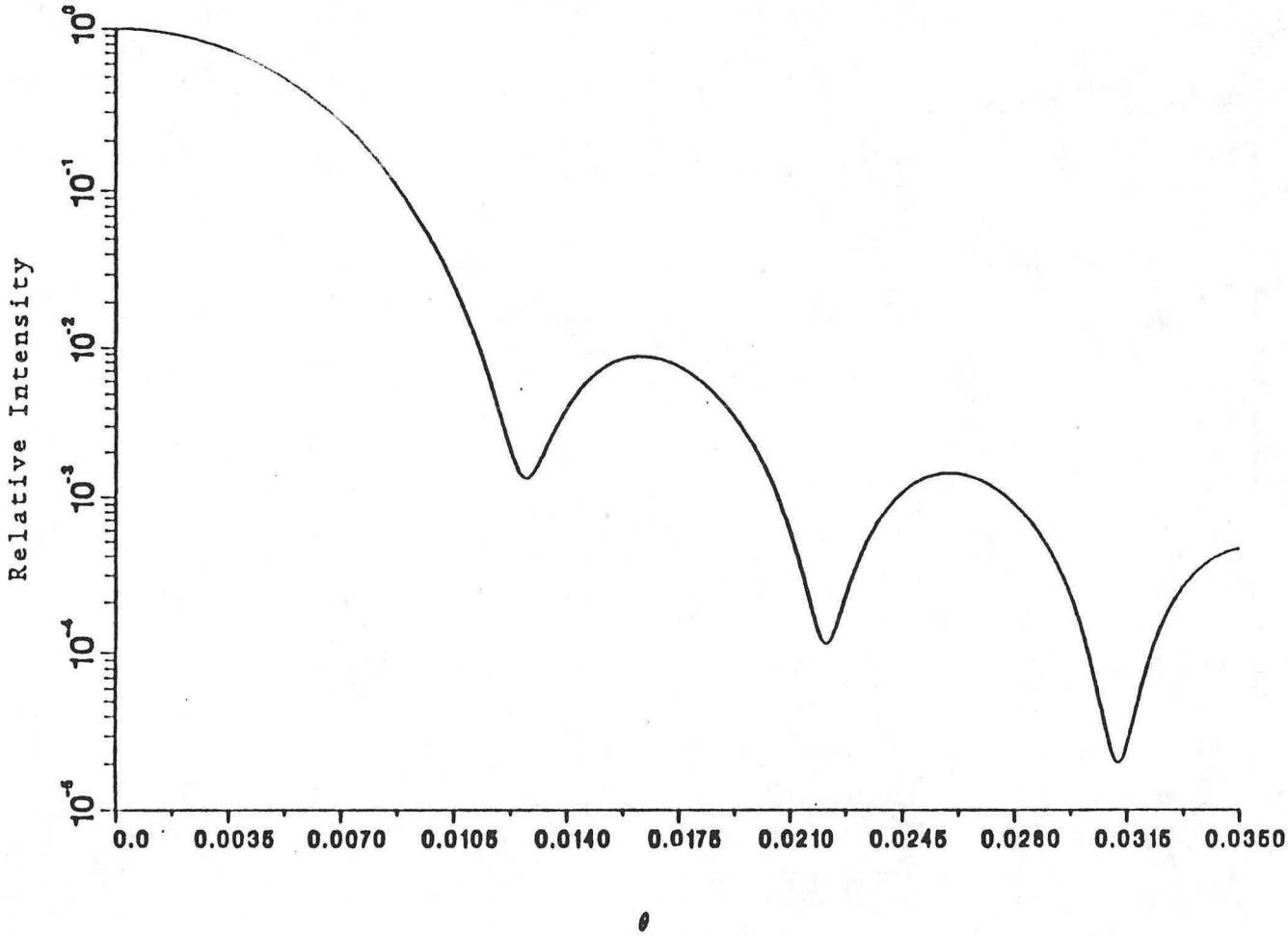

Figure 28: Calculated intensity distribution vs. axial angle ϑ for an unordered array of spheres of 496nm diameter.

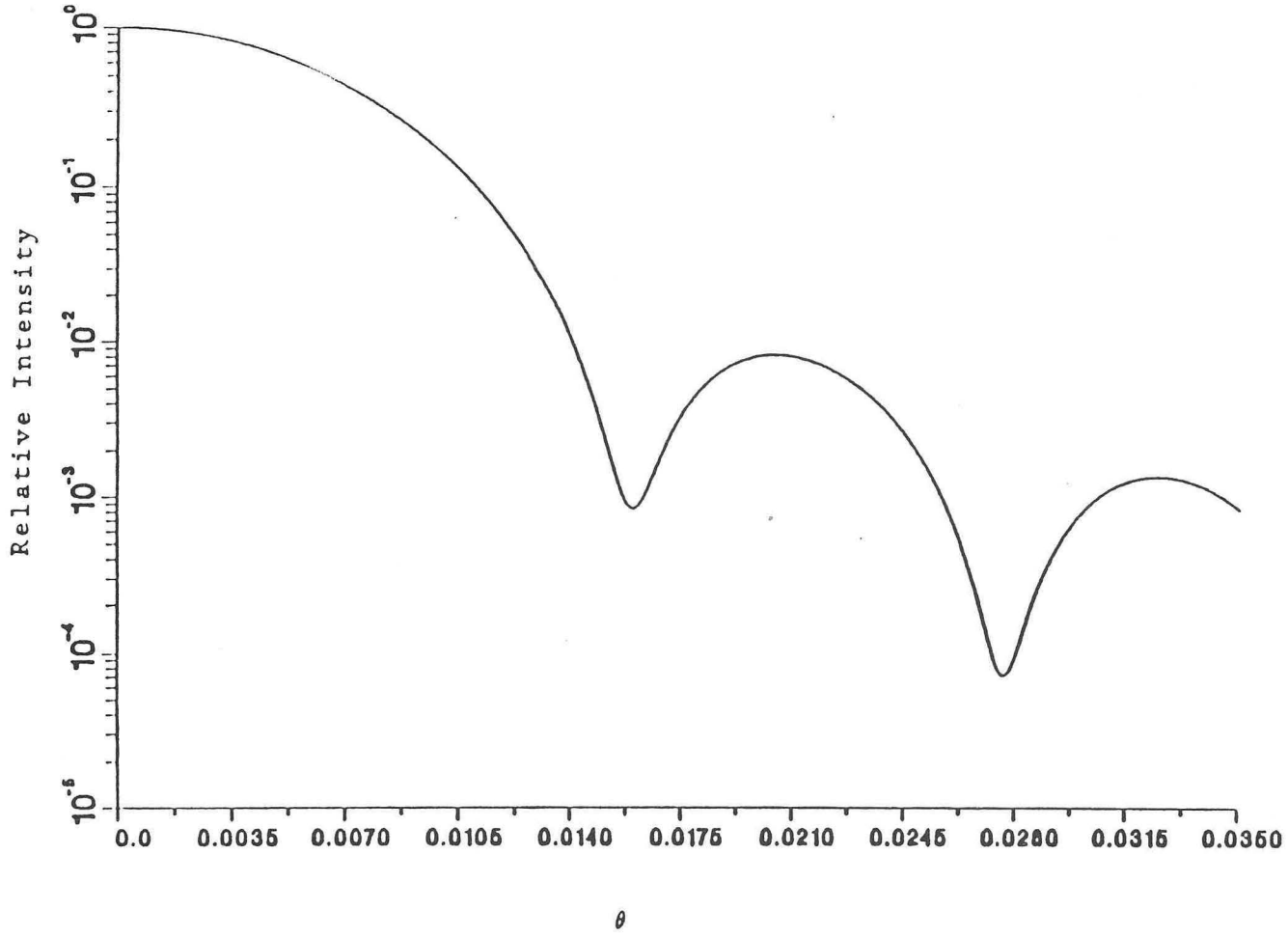

Figure 29: Calculated intensity distribution vs. axial angle ϑ for an unordered array of spheres of 398nm diameter.

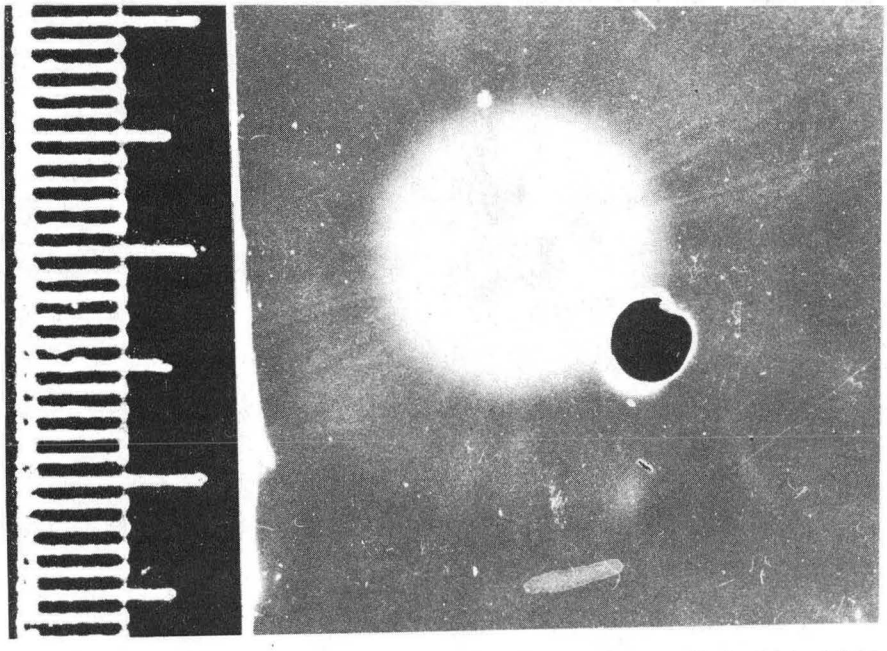

XBB 893-1561

Figure 30: Resulting intensity distribution from a 5.0 hour exposure with C-K radiation and 398nm diameter spheres.

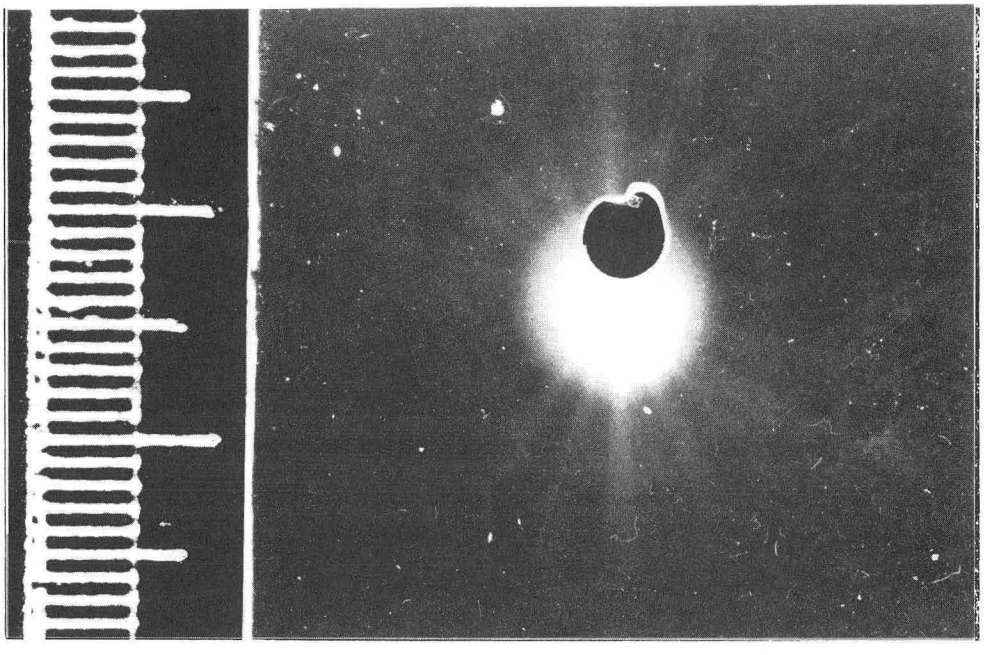

XBB 893-1562

Figure 31: Resulting intensity distribution from a 2.5 hour exposure with C-Kα radiation and 597 nm diameter spheres

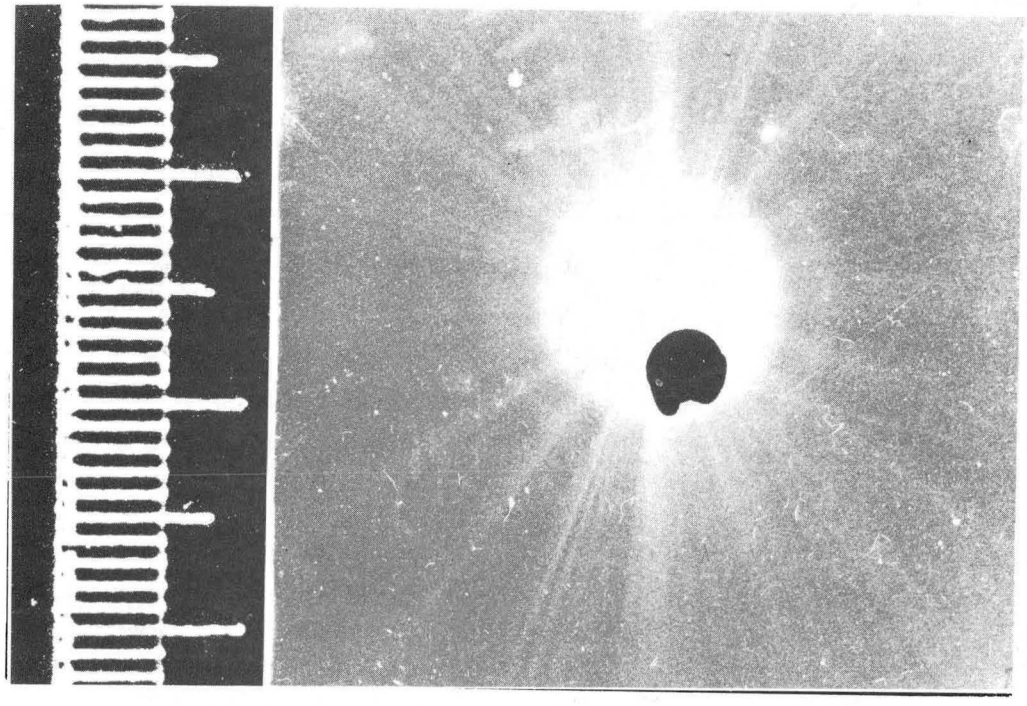

XBB 893-1563

Figure 32: Resulting intensity distribution from a six hour exposure with C-Kα radiation and 895 nm diameter spheres

Table 1: Measured and calculated radii of first and second secondary maxima of diffraction patterns from lattice structures of spheres of different diameters.

Diameter of Spheres	Radius of Maxima	Calculated Radius
597 nm	0.4 cm	0.42 cm
	0.7 cm	0.73 cm
895 nm	0.3 cm	0.28 cm
	0.5 cm	0.49 cm

Table 2: Measured and calculated radii of first secondary maximum of diffraction patterns from unordered arrays of spheres of various diameters.

Diameter of Spheres	Radius of Maximum	Calculated Radius
398 nm	1.0 cm	0.98 cm
496 nm	0.8 cm	0.78 cm
597 nm	0.6 cm	0.65 cm
895 nm	0.4 cm	0.42 cm

Conclusion

This work illustrates that small angle soft x-ray scattering allows the observation of structures whose size is intermediate between that observable in a light microscope (> 1 micron) and those determined by other x-ray techniques (~ 10 Å). Using polystyrene spheres, two methods of diffracting x-rays were used. One had a relatively low effective sample area and hence did not produce an observable pattern. The other method, which used a C-W multi-layer mirror of spacing 44.8 A to focus the radiation, imaged the x-ray source onto the sample. This method results in an effective sample area of approximately 2000 times the first effective sample area. Because of the large number of spheres which were diffracting the radiation, diffraction patterns were observed with this method. Patterns arising from lattice structures of spheres and also from random arrays of spheres were measured, and compared well with the calculated pattern shapes and sizes.

The success of second method indicates the development of a novel technique of sizing particles. Specifically, since large samples areas may be illuminated with low intensity radiation, biological particles may be sized and their structure determined without extensive radiation damage to the particles, and under practical conditions integral to small angle scattering. Combining this technique with high flux from proposed 1-2 GeV synchrotron radiation sources, dilute concentration of biological materials and changes in periodic structures like muscle tissue can be studied. Subsequent work will finally allow observation of biological particles in controlled environments, and thus a better understanding of biological processes.

Acknowledgements

We would like to thank P. Batson and R. Delano for their invaluable assistance in designing and fabricating the apparatus; R. Falcone, S. Rothman and K. McQuaid for their encouragement; J. Bastacky for the electron micrograph measurements; and E. Essman and M. Thomas for their assistance in preparation of this report. This work was supported by the U.S. Department of Energy, under contract no. DE-AC03-76SF00098.

APPENDIX 1

A Printout of the Program which Numerically Calculates the Normalized Intensity Distribution of Radiation Scattered From a Sphere

```
      Program Amp

C     This program calculates the value of the intensity
C     function of light scattered by a sphere.

c     version E (4/26/88)


      complex sum, im2, im, ro, index
      real dtau, tau, zmin, zmax, dz, dxi, lambda, dist, diam, rad
     *         ,aint

      pi = 4.0 * atan(1.0)
      im = (0.,1.)
      im2 = (1.,0.)


      type *, ' PROGRAM AMP:  This program calculates the '
      type *, ' intensity of the scattered light '

      type*, ' '
      type*, ' Enter the complex value of the index of refraction '
      type*, '                                n = (Re, Im) '
      read (5,*) index

      type*, ' Enter the diameter of the spheres '
      read(5,*) diam

      type*, ' Enter the wavelength of the incident light '
      read(5,*) lambda

      type*, ' Enter the distance from the mirror to film '
      read(5,*) dist

      x = pi*diam/lambda
      ro = 2*x*(index - 1.)
d     type*, ro, x

      type*, ' Enter the minimum and maximum values of theta '
      read(5,*) thetamin, thetamax

      type*, ' Enter the distance between theta points on this range '
      read(5,*) dtheta

      type*, ' Enter the number of steps in the tau integral '
      type*, '                    [0 to pi/2] '
      read(5,*) ntpnts

      type*, ' Enter the number of steps in the Bessel function integral '
      type*, '                   [0 to 2pi] '
      read(5,*) nbpnts

      zmin = x*thetamin
      zmax = x*thetamax
      dz = x*dtheta

      nzpnts = nint ( (zmax - zmin)/dz )
```

```
      dtau = 0.5*pi/ntpnts


      open (unit = 7, file = 'Intensity.dat', status = 'new')

      do 10 i = 0, nzpnts

      z = zmin + i * dz

      sum  = 0.
      do 20 j = 1, ntpnts

              taul = j * dtau
              tau = (j - 1)*dtau
              sum = sum + 0.5 *dtau * sin(tau) * cos(tau) *
     *                bessel (0,nbpnts,z*cos(tau)) *
     *                 (1.0 - cexp( -im*2* ro*sin(tau) ) )

              sum = sum + 0.5 *dtau * sin(taul) * cos(taul) *
     *                 bessel (0,nbpnts, z*cos(taul)) *
     *                 (1.0 - cexp( -im*2* ro*sin(taul) ) )

20    continue

d     type*, sum

      rad = z*dist/x
      aint = sum * conjg (sum)
      write (7,*) z/x, aint
      type*, z, z/x, rad, aint

10    continue

      close (unit = 7)

      stop
      end
```

```
      Real Function Bessel (m, nsteps, vo)

C     This program calculates the Bessel function for a set of
c     data points, of INTEGER order m.


      real dv, vo, pi
      integer m

      pi = 4.0*atan (1.0)
      dv = pi/nsteps

      bessel = 0.

      do 20 j = 1, nsteps

              a = j * dv
              al = (j - 1)*dv
              f = cos(m*a - vo*sin(a))
              f1 = cos(m*al - vo*sin(al) )
              bessel = bessel + 0.5* (f + f1) * dv

20    continue

      bessel = bessel/pi

      return
      end
```

APPENDIX 2

A Printout of the Program which Numerically Calculates the Normalized Intensity Distribution of Radiation Scattered From a Lattice of Spheres

```
      PROGRAM ARRAY

C     This program calculates the modulating function
C     on a single particle intensity for a hexogonal array,
C     and multiplies it by the single particle function,
C     which should be calculated using the program "amp".

C     version G (5/7/88)

      character*30 file1, file2


      pi = 4.0*atan(1.0)

      type*, ' Enter phi [IN DEG]'
      read(5,*) phi

      phi = phi*pi/180.

      type*, ' Enter the indices of the corner sphere '
      type*, ' N1, M1 (BOTH ODD--see paper) '
      read(5,*) nred, mred

      type*, ' Enter the wavelength of the incident light '
      read(5,*) wlambda

      wnumber = 2 * pi / wlambda

      type*, ' Enter the diameter of the spheres '
      read(5,*) diam

      type*, ' Enter the name of the file containing the '
      type*, ' single particle function '
      read (5,77) file1

      type*, ' Choose the output file name '
      read(5,77) file2

      open (unit = 8, file=file1, status='OLD',readonly)
      open (unit = 7, file=file2, status='NEW')


      write(7,*) 'PHI = ', PHIMIN

      write(7,*) ' DIMENSION = ', nred, mred

78    continue

      read(8,*, end=1) theta, sfunc

      z = 0.5*wnumber * diam * sin(theta)

      arg1 = z * cos(phi)
      arg2 = z * sin(phi) * sqrt(3.0)

C     The computer cannot take the limit sin(x)/x = 0 as
C     x goes to 0, so set up the conditions so that
```

```
C       it does not have to.

        if (sin(arg1) .eq. 0 .and. sin(arg2) .eq. 0) then

        function = 2*( 0.5*(nred + 1)*0.5*(mred + 1) )**2

        else if(sin(arg1) .eq. 0 .and. sin(arg2) .ne. 0) then

        function = 0.5* nred *sin( 0.5*(mred+1)*arg2) /
     *          sin(arg2)
        function = (function**2)*(1 + cos(arg2))

        else if (sin(arg1) .ne. 0 .and. sin(arg2) .eq. 0)then

        function = 0.5* mred *sin( 0.5*( nred+1) *arg1)
     *          /sin(arg1)
        function = (function**2)*(1 + cos(arg1))

        else if (sin(arg1) .ne. 0 .and. sin(arg2) .ne. 0) then


        function = sin(0.5*(nred+1) *arg1) * sin( 0.5*(mred+1) *arg2)

        function = function / (sin(arg1)*sin(arg2))

        function = (function**2)*(1 + cos(arg1 + arg2))


        end if

C       multiply this "lattice" intensity by the "single
C       particle" intensity

        function = function * sfunc

        type*, ' THETA = ', THETA, ' PHI = ', PHI, ' FUNC = ',FUNCTION

2       continue

        write(7,*) theta, function

        goto 78

1       continue

        close (UNIT=7)
        close (unit=8)

        stop

77      format (a30)

        end
```

References

1. B.L. Henke, J.W.M. DuMond, J. Appl. Phys., 26, 7 (1955)

2. H.H. Paradies, Opt. Eng. 21, 894 (1982)

3. H.C. van de Hulst, Light Scattering by Small Particles (Dover, New York, 1981)

4. E. Hecht, Optics (Addison-Wesley, Reading, MA, 1987)

5. B.L. Henke, P. Lee, T.J. Tanaka, R.L. Shimabukuro, B.K. Fujikawa, Atomic Data and Nuclear Tables, 27, 1 (1982)

6. R.C.C. Perera, PhD Thesis (University of Hawaii, May 1978)

7. B.L. Henke, F.G. Fujiwara, M.A. Tester, C.H. Dittmore, M.A. Palmer, J. Opt. Soc. Am. B, 1, 6 (1984)

8. Mention of the name Duke Scientific in no way constitutes an endorsement for their products.

9. J.H. Underwood, Rev. Sci. Instr., 47, 5 (1976)

LAWRENCE BERKELEY LABORATORY
TECHNICAL INFORMATION DEPARTMENT
1 CYCLOTRON ROAD
BERKELEY, CALIFORNIA 94720